Cholinergic projections to the substantia nigra reticulata inhibit dopamine modulation of basal ganglia through the M4 muscarinic receptor

Mark S. Moehle[1,*], **Tristano Pancani**[1,*], **Nellie Byun**[1], **Samantha E. Yohn**[1], **George H. Wilson III**[2], **Johnathan W. Dickerson**[1], **Daniel H. Remke**[1], **Zixiu Xiang**[1], **Colleen M. Niswender**[1,3], **Jurgen Wess**[4], **Carrie K. Jones**[1], **Craig W. Lindsley**[1], **Jerri M. Rook**[1], and **P. Jeffrey Conn**[1,3,†]

[1]Vanderbilt Center for Neuroscience Drug Discovery and Department of Pharmacology

[2]Vanderbilt University Institute of Imaging Science, Vanderbilt University, Nashville, TN

[3]Vanderbilt Kennedy Center, Vanderbilt University School of Medicine, Nashville, TN

[4]Molecular Signaling Section, Laboratory of Bioorganic Chemistry, NIDDK, NIH, Bethesda, MD

Summary

Cholinergic regulation of dopaminergic inputs into the striatum is critical for normal basal ganglia (BG) function. This regulation of BG function is thought to be primarily mediated by acetylcholine released from cholinergic interneurons (ChIs) acting locally in the striatum. We now report a combination of pharmacological, electrophysiological, optogenetic, chemogenetic and functional magnetic resonance imaging studies suggesting extra-striatal cholinergic projections from the pedunculopontine nucleus to the substantia nigra pars reticulata (SNr) act on muscarinic acetylcholine receptor subtype 4 (M_4) to oppose cAMP-dependent dopamine receptor subtype 1 (D_1) signaling in presynaptic terminals of direct pathway striatal spiny projections neurons. This induces a tonic inhibition of transmission at direct pathway synapses and D_1-mediated activation of motor activity. These studies provide important new insights into the unique role of M_4 in regulating BG function and challenge the prevailing hypothesis of the centrality of striatal ChIs in opposing dopamine regulation of BG output.

[†]To whom correspondence should be addressed and lead contact: P. Jeffrey Conn, Lee Limbird Professor of Pharmacology, Director, Vanderbilt Center for Neuroscience Drug Discovery, Vanderbilt University, 1205 Light Hall, Nashville, TN 37232, jeff.conn@vanderbilt.edu.
[*]These authors contributed equally

Introduction

The striatum is the primary gateway to the basal ganglia (BG) motor circuit and plays a critical role in regulating motor function, motivation, habit formation, and cognition (Albin et al., 1989; Alexander et al., 1990; Graybiel, 2008; Pisani et al., 2005). Dopaminergic inputs to the striatum from the substantia nigra pars compacta (SNc) play an important role in regulating striatal output and BG-influenced behaviors (Beaulieu and Gainetdinov, 2011). In addition, dopamine (DA) signaling in the striatum is dysregulated in multiple movement disorders and psychiatric illnesses (Albin et al., 1989; Goodchild et al., 2013; Wichmann and DeLong, 1996).

A major regulator of DA signaling in the BG is acetylcholine (ACh), acting through muscarinic acetylcholine receptors (mAChRs) and nicotinic acetylcholine receptors (nAChRs) (Bonsi et al., 2011; Picciotto et al., 2012). nAChRs are non-selective cation channels that have profound effects on DA release (Cachope and Cheer, 2014), and have been implicated in multiple disorders where DA is disturbed (Crunelle et al., 2010). mAChRs are G protein-coupled receptors that also modulate DA release and signaling (Kruse et al., 2014; Shin et al., 2015; Zhang et al., 2002). For instance, mAChR agonists inhibit DA release and suppress behavioral effects of psychostimulants that act by increasing DA levels (Bendor et al., 2010; Foster et al., 2014; Foster et al., 2016; Starke et al., 1989). Furthermore, disturbances of mAChR signaling have been implicated in many neurologic and neuropsychiatric disorders that are thought to involve changes in DA signaling (Aosaki et al., 2010; Holt et al., 1999; Kataoka et al., 2010; Pisani et al., 2007).

Cholinergic interneurons (ChIs) in the striatum are large, aspiny, tonically-active interneurons that are thought to be central to the ability of ACh to modulate the BG (Holt et al., 1999; Pisani et al., 2007; Tanimura et al., 2017). However, recent studies suggest that non-striatal sources of ACh may also regulate BG output. Hindbrain cholinergic nuclei of the pedunculopontine nucleus (PPN) and laterodorsal tegmental nucleus (LDT) project to BG nuclei and brain regions that regulate the BG such as the SNc (Dautan et al., 2014; Saper and Loewy, 1982). Optogenetic or electrical activation of projections from either the PPN or LDT can modulate locomotion, reward, and gait (Wen et al., 2015; Xiao et al., 2015), suggesting that cholinergic neurons in the hindbrain may also regulate the BG output. However, the sites of action of these hindbrain cholinergic nuclei and the AChR subtypes they modulate are not well understood.

In recent years, M_4 has emerged as the primary mAChR subtype responsible for regulating DA signaling in the striatum (Conn et al., 2009), as psychomotor effects of non-selective mAChR agonists are diminished in M_4 knockout (KO) mice (Gomeza et al., 2001; Guo et al., 2010). Additionally, selective positive allosteric modulators (PAMs) of M_4 decrease amphetamine-induced increases in extracellular DA in the striatum and functional magnetic resonance imaging (fMRI) studies reveal that M_4 PAMs induce a profound reduction in amphetamine-induced activation of the striatum and other forebrain regions (Byun et al., 2014). Furthermore, M_4 PAMs reduce effects of DA-releasing stimulants on locomotor activity and other behavioral responses (Brady et al., 2008; Bubser et al., 2014; Byun et al., 2014; Dencker et al., 2012; Foster et al., 2016). Recent studies also suggest that M_4 PAMs

act in part, by inhibition of DA release in the striatum by release of an endocannabinoid from spiny projection neurons (SPNs) and activation of presynaptic cannabinoid receptor 2 (CB_2) on DA terminals (Foster et al., 2016).

While the behavioral effects of M_4 PAMs are likely to be partially mediated by inhibition of DA release, M_4 is highly expressed in SPNs that express the DA receptor subtype 1 (D_1); forming the direct pathway (D_1-SPNs) and send inhibitory projections to the substantia nigra pars reticulata (SNr)(Hersch et al., 1994; Levey et al., 1991). Activation of D_1-SPNs in the striatum leads to GABA release, inhibition of GABAergic SNr projection neurons, disinhibition of the thalamus, leading to excitation of the cortex and facilitating goal-directed movement. Interestingly, D_1 activates a unique G protein in D_1-SPNs, $G\alpha_{olf}$, that couples D_1 to activation of adenylyl cyclase (AC), formation of cAMP, and activation of protein kinase A (Corvol et al., 2007; Herve, 2011; Zhuang et al., 2000). This signaling pathway is critical for many of the behavioral actions of amphetamine that are reversed by M_4 PAMs (Drago et al., 1998; Zhuang et al., 2000). The M_4 receptor couples to $G\alpha_i$, which inhibits AC and can counteract the effects of D_1/$G\alpha_{olf}$ activation (Onali and Olianas, 2002), raising the possibility that M_4 PAMs may also directly inhibit D_1 signaling in D_1-SPNs by inhibition of cAMP formation. Here, we report that M_4 PAMs reverse increases in locomotor activity induced by a D_1 agonist, which cannot be mediated by inhibition of DA release. Furthermore, pharmacological, genetic, molecular, and cellular studies reveal that this response is mediated by inhibition of D_1 signaling in D_1-SPNs through opposing actions on AC. Surprisingly, the primary action of M_4 PAMs on D_1 signaling is not in the striatum, but on GABAergic terminals of D_1-SPNs in the SNr. This finding challenges the traditional view that cholinergic regulation of BG function is mediated exclusively through ACh released from ChIs, and highlights an important role for extra-striatal sources of ACh projecting to other BG nuclei, which may also play a critical role in cholinergic regulation of DA signaling and activity through the BG motor circuit (Aosaki et al., 1995; Bolam et al., 1984; Bonsi et al., 2011; Hersch et al., 1994; Wilson et al., 1990).

Results

D_1 agonists induce hyperlocomotion which is reversed by M_4 PAM administration

Previously, we reported that the M_4 PAM VU0467154 reversed hyperlocomotion induced by amphetamine, a stimulant that acts by increasing extracellular DA. These studies also provided evidence that this effect is partially mediated by inhibition of DA release in the striatum (Bubser et al., 2014; Foster et al., 2016). To determine whether the M_4 PAM can have actions that are independent of DA release, we studied the effect of VU0467154 on hyperlocomotion induced by the D_1-selective agonist SKF82958. Consistent with previous reports, SKF82958 (1 mg/kg, intraperitoneal (i.p.)) induced a robust increase in locomotor activity in wildtype (WT) mice (Figure 1 A-B, Figure S1, one-way ANOVA with Tukey's post-hoc test, $p<0.001$). Mice pre-treated with VU0467154 (3 - 30 mg/kg, i.p.) exhibited a dramatically reduced hyperlocomotor response to SKF82958 (Figure 1 A-B, Figure S1 A, one-way ANOVA with Tukey's post-hos test, $p<0.001$ (3 and 30 mg/kg), $p<0.01$ (10mg/kg)), suggesting that M_4 PAMs can reduce responses to direct D_1 activation.

To further assess the mechanism by which M_4 PAMs may reduce responses to the D_1 agonist, we used a previously characterized mouse in which M_4 receptors are selectively deleted from D_1-expressing neurons (Jeon et al., 2010). These D_1-M_4 KO mice display a hyperlocomotor response to SKF82958 (1 mg/kg, i.p.) that is similar to that of WT animals. However, VU0467154 (3 - 30 mg/kg, i.p., 10% Tween 80) failed to reduce the response to SKF82958 in D_1-M_4 KO mice (Figure 1C-D, Figure S1 B, one-way ANOVA with Tukey's post-hoc test, $p>0.05$).

In order to determine whether the M_4 PAM has actions on motor function without administration of a D_1 agonist, we administered VU0467154 (3 - 30 mg/kg, i.p) to WT mice 30 minutes prior to testing. Animals administered VU0467154 showed significantly decreased spontaneous locomotion compared to vehicle controls (Figure S1C, D; one-way ANOVA with Tukey's post-hos test, $p<0.05$). This suggests that M_4 activity may regulate direct pathway activity in baseline states, and raises the possibility that there is behaviorally relevant tonic inhibition of D_1-SPNs by M_4.

M_4 receptors co-localize with D_1-SPN terminals in the SNr

Previous studies revealed a diverse expression pattern of M_4 throughout the brain, with particularly robust expression in the striatum, cortex, and the hippocampus (Levey, 1991). In the striatum, M_4 is found on glutamatergic terminals, ChIs, and D_1-SPNs (Levey, 1991; Hersch, 1994). In addition, M_4 activation can inhibit D_1/cAMP-mediated responses in the striatum (Jeon et al., 2010; Sánchez-Lemus and Arias-Montaño, 2006), suggesting inhibition of D_1 signaling at the level of the striatum could contribute to the ability of M_4 PAMs to inhibit behavioral responses to the D_1 agonist. However, direct site infusion of D_1 modulators into the SNr provide intriguing evidence that activation of D_1 on D_1-SPN terminals in the SNr also contribute to the effects of D_1 activation on locomotor activity (Trevitt et al., 2001; Trevitt et al., 2002). To study the expression patterns of M_4, we utilized a reporter mouse that expresses the red fluorescent protein td-Tomato in D_1-SPNs combined with previously characterized antibodies (Hersch et al., 1994; Levey et al., 1991). Similar to previous reports, M_4 puncta (green) can be seen in td-Tomato positive cell bodies, suggesting likely M_4 expression on D_1-SPNs (Figure S2). Diffuse M_4 puncta were also observed throughout the striatum that sometimes co-localize with td-Tomato, suggesting that M_4 is present on the dendrites of D_1-SPNs as well as other neuropil, likely cortico-striatal projections (Figure S2). In the striatum, M_4 staining was largely absent in an M_4 KO animal (Figure S2). In the SNr, robust M_4 staining was observed in td-Tomato positive puncta, suggesting that M_4 is robustly co-expressed with a marker for D_1-SPN terminals (Figure S2). We could not determine whether the M_4 staining on cell bodies in the SNr was specific for M_4, as equally intense staining was observed only in the cell bodies of M_4 KO animals. However, loss of staining associated with D_1 terminals in M_4 KO suggests that M_4 is localized in terminal regions of D_1-SPNs.

Cholinergic fibers in the SNr originate from the hindbrain cholinergic nuclei

To determine the source of ACh in the SNr, we utilized retrobeads which, when injected into a brain region, are retrogradely transported back to the soma of cells that project to that brain region (Katz et al., 1984). We performed focal injections of these beads into the SNr (Figure

S3A). When staining for cholinergic cells using VAChT antibody and a coronal sectioning technique, we could distinguish the LDT from the PPN (Figure S3B). In line with previous reports (Beninato and Spencer, 1987), robust bead uptake can be seen in cholinergic cells of the PPN but not the LDT, suggesting that the PPN is the main source of ACh in the SNr (Figure S3C). Additionally, when staining for VAChT in the SNr, cholinergic fibers can be visualized, and their density estimated at a modest density of ~6 fibers/100 μm^2 (Figure S3D).

D_1 agonists and M_4 PAMs regulate mIPSC frequency in GABAergic cells of the SNr

To assess the functional effects of D_1 and M_4 activation at the level of D_1-SPN terminals in the SNr, we performed whole-cell patch clamp recordings from GABAergic cells of the SNr in the presence of CNQX, AP5, and TTX, to isolate miniature inhibitory post synaptic currents (mIPSCs). GABAergic cells were distinguished from DA cells of the SNr through intrinsic firing rates of the cells and through membrane properties (Figure S4A). Bath application of 10 μM SKF82958 caused a leftward shift in cumulative probability of release with a ~ 40% increase in mIPSC frequency (Figure 2A-C, Table S1 Wilcoxon signed rank test, p<0.05) without changes in mIPSC amplitude (Table S1, Wilcoxon signed rank test, p>0.05). Additionally, we confirmed that these responses are mediated by $GABA_A$ with bath application of 50 μM of the $GABA_A$ antagonist bicuculline, which abolished detectable events (Figure S4B). Taken together, these results confirm previous reports that D_1 activation robustly increases GABA release probability from D_1-SPN terminals onto SNr neurons (Radnikow and Misgeld, 1998; Trevitt et al., 2002).

Pre-treatment with the muscarinic agonist oxotremorine-M (Oxo-M; 10 μM) completely eliminated the effect of SKF82958 on mIPSCs. The M_4-selective PAM VU0467154 (10 μM) mimicked the effect of Oxo-M (Table S1, Figure 2 A-C; one-way ANOVA with Tukey's post-hoc test, p<0.05). Lower concentrations of VU0467154 (5 μM) or Oxo-M (2 μM) failed to reduce the effects of 10 μM SKF82958 (Table S1, Figure S3C-D, Figure 2A-C, one-way ANOVA with Tukey's post-hoc test, p>0.05). However, when combined, 5 μM VU0467154 and 2 μM Oxo-M significantly blocked the effects of 10 μM SKF82958 (Table S1, Figure 2A-C, one-way ANOVA with Tukey's post-hoc test, p<0.05). This ability of a low concentration of VU0467154 to potentiate the response to a threshold concentration of Oxo-M is consistent with the M_4 PAM mechanism. These findings were confirmed in slices warmed to 30°C (Figure S4F).

In addition to evaluating effects of VU0467154 on the response to an exogenous agonist, we also performed studies in slices with channel rhodopsin 2 (ChR2) selectively expressed in choline acetyltransferase (ChAT)-positive cholinergic neurons to evoke ACh release. Optical stimulation of cholinergic afferents using 10 Hz, 5 ms, 470 nm light pulses reduced baseline mIPSC frequency by~20%, which is similar in magnitude to the effect of 10μM Oxo-M (Figure S4E). At this intensity, optical stimulation alone did not inhibit the mIPSCs when stimulated with SKF82958 (Table S1, Figure 2D-F, one-way ANOVA with Tukey's post-hoc test, p>0.05), providing an appropriate optical stimulation intensity for evaluation of the effects of the M_4 PAM. However, when combined with a concentration of VU0467154 (5μM) that had no effect in the absence of optical stimulation, this intensity induced a robust

inhibition of the effects of SKF82958 on mIPSC frequency (Tables S1, Figure 2D-F, one-way ANOVA with Tukey's post-hoc test, p<0.01). These data suggest that that ACh released in the SNr inhibits mIPSCs from D_1-SPNs in the SNr and that the effect of activation of cholinergic afferents is potentiated by selective M_4 PAMs.

Genetic deletion of M_4 in D_1-SPNs blocks pharmacological inhibition of D_1 mediated responses

To test the hypothesis that M_4 expressed in D_1-SPNs is responsible for the inhibition of D_1-induced increases in GABA release probability, we performed identical studies in slices from D_1- M_4 KO mice. Bath application of 10 μM SKF82958 significantly increased mIPSC frequency compared to baseline (Table S1, Figure 3A-C, Wilcoxon signed rank test, p<0.01). However, D_1-mediated increases in mIPSC frequency were not blocked by 10 μM Oxo-M, 10 μM VU0467154 or a combination of subthreshold concentrations of VU0467154 (5 μM) and Oxo-M (2 μM) (Table S1, Figure 3A-C, one-way ANOVA with Tukey's post-hoc test, p>0.05) in D_1-M_4 KO mice. Again, neither SKF82958 nor the muscarinic agents altered mIPSC amplitude (Table S1, Wilcoxon signed rank test, p>0.05), and all events were blocked with 50 μM bicuculline (Figure S4G). Control studies were performed in which we found that bath application of 10 μM baclofen, a $GABA_B$ agonist, induced a similar decrease in mIPSC frequency in slices from WT and D_1- M_4 KO animals (Figure S4H-J, two-way t-test, p>0.05). These data suggest that the D_1-SPN terminals in D_1-M_4 KO mice were not altered in a homeostatic manner, and that mIPSCs could be inhibited by activation of another G protein-coupled receptor (Borgkvist et al., 2015).

Importantly, D_1-M_4 KO mice may bear deletions of M_4 from any neurons that express both M_4 and the D_1 receptor. Thus, it is conceivable that deletion of M_4 in other cells within the SNr in D_1-M_4 KO mice could contributes to the loss of responses to M_4 activation in these mice. To control for this, we performed additional studies to confirm that the response to mAChR agonists and M_4 PAMs in the SNr could be rescued by restoring M_4 signaling in striatal neurons of D_1-SPN KO mice by stereotaxic injection of a viral construct encoding the hM_4Di designer receptor exclusively activated by a designer drug (DREADD) into the striatum (Krashes et al., 2011). This DREADD is a modified M_4 receptor that no longer binds ACh, but can be selectively activated by clozapine-N-oxide (CNO), an inactive metabolite of clozapine. Bath application of 10 μM CNO to slices from animals expressing the hM_4Di DREADD induced a robust inhibition of SKF82958-induced increases in mIPSC frequency (Table S1, Figure 3 A-C, one-way ANOVA with Tukey's post-hoc test, p<0.05). Additionally, application of 10 μM CNO alone produced a profound decrease in mIPSC frequency, suggesting that replacing M_4 with an M_4 DREADD to restore M_4-dependent signaling is sufficient to decrease D_1-SPNs activity (Table S1, Figure 3 A-C Wilcoxon signed rank test, p<0.05). Taken together, these studies suggest that selective activation of M_4 inhibits D_1-induced increases in transmission at striato-nigral synapses by actions in D_1-SPN terminals.

M_4 may tonically inhibit mIPSCs in D_1-SPNs

VU0467154 is a prototypical M_4 PAM that does not induce significant activation of M_4 by itself, but acts by potentiating the response to ACh (Bubser et al., 2014). Thus, the finding

that VU0467154 alone inhibits mIPSCs raises the possibility that ACh exerts a tonic inhibition of mIPSC frequency that is potentiated by the M_4 PAM. Consistent with this, there was an approximate doubling of mIPSC frequency from ~4 Hz to ~8 Hz in D_1-M_4 KO mice relative to D_1-Cre and WT mice (Table S1, Figure 4A, B, one way ANOVA with Tukey's post-hoc test, $p<0.001$). Furthermore, bath application of the non-subtype-selective mAChR antagonist scopolamine (10 μM) or the M_4-selective toxin mamba toxin 3 (MT3; 1 μM) induced an increase in mIPSC frequency (Table S1, Wilcoxon signed rank test, $p<0.01$, Figure 4C-E). Conversely, application of 10 μM VU0467154 induced a modest decrease in mIPSC frequency (Table S1, Wilcoxon signed rank test, $p<0.05$, Figure 4C-E). When these agents are applied to slices from D_1-M_4 KO mice their effect is absent or greatly reduced (Table S1, Figure 4C-E, one way ANOVA with Tukey's post-hoc test, $p<0.001$).

To directly determine whether release of ACh from the PPN onto M_4 receptors induces a tonic inhibition of D_1-SPNs, we utilized a cre-dependent, constitutively active caspase 3 virus injected into the hindbrain of ChAT-Cre positive animals (Yang et al., 2013). Injection of the virus greatly reduced cholinergic cells in the hindbrain (Figure 4F). In *ex vivo* recordings from slices prepared from caspase3 or control virus injected ChAT-Cre mice, GABAergic cells of the SNr from cholinergic depleted animals had a higher baseline mIPSC frequency than control virus injected ChAT-Cre animals (Figure 4F-H, Table S1, Mann-Whitney test, $p<0.05$) and were no longer responsive to MT3 (Figure 4G). Taken together, these data suggest that there is a high basal activity of M_4 and that cholinergic projections from the hindbrain exert an M_4-mediated inhibition of transmission at GABAergic terminals from D_1-SPNs.

D_1 and M_4 converge on AC to alter mIPSC frequency

D_1 couples to $G\alpha_{olf}$, which activates AC in D_1-SPNs, in a manner similar to $G\alpha_s$ in other cell types (Zhuang et al., 2000). Thus, it is possible that D_1 increases mIPSCs through a cAMP-dependent mechanism and that M_4 inhibits D_1 responses by $G\alpha_{i/o}$-mediated inhibition of AC and production of cAMP. We first perfused SNr slices with 50 μM of the AC activator forskolin (FSK) to increase intracellular cAMP levels. In both WT and D_1-M_4 KO animals, bath application of FSK resulted in a significant increase in mIPSC frequency (Figure S5, Wilcoxon signed rank test, $p<0.05$). Additionally, 10 μM Oxo-M, 10 μM VU0467154, or a combination of subthreshold concentrations of or Oxo-M and VU0467154 blocked FSK-induced increases in mIPSC frequency (Figure S5A,B one-way ANOVA with Tukey's post hoc test, $p<0.01$) but not D_1-M_4 KO animals (Figure S5C,D one-way ANOVA with Tukey's post hoc test, $p>0.05$).

To further test the hypothesis that the effects of M_4 on D_1 are mediated by reciprocal effects on AC activity, we utilized a β2-Opto-XR optogenetic construct injected into the striatum. This construct activates AC and accumulation of cAMP (Siuda and McCall, 2015). Since D_1-SPNs, but not SPNs of indirect pathway, project to the SNr, our coronal sectioning technique provided sections in which the construct is only expressed in D_1-SPN terminals in the SNr (Figure 5A, B). Activation of AC by optical stimulation in SNr increased mIPSC frequency in both WT and D_1-M_4 KO animals (Table S1, Figure 5C-F, Wilcoxon signed rank test, $p<0.001$). Also, consistent with our other studies, the increase in mIPSC frequency

due to β2-Opto-XR stimulation could be blocked with 10 μM Oxo-M or a combination of 2 μM Oxo-M and 5 μM VU0467154 in WT (TableS1 Figure 5C, D, one-way ANOVA with Tukey's post hoc test, p<0.001) but not D_1-M_4 KO mice (Table S1, Figure 5E, F, one-way ANOVA with Tukey's post hoc test, p>0.05). Additionally, WT or D_1-M_4 KO mice injected with an enhanced yellow fluorescent protein (eGFP) control vector did not display significant increases in mIPSC frequency (Tables S1, Figure 5C-F, Wilcoxon signed rank test, p>0.05). Taken together, these data support the hypothesis that M_4 and D_1 have opposing actions on AC in D_1-SPN terminals in the SNr to induce reciprocal effects on D_1-SPN output.

M_4 suppresses D_1-SPN-induced BG activation at the level of the SNr

We previously reported that M_4 PAMs inhibit DA release in the striatum (Foster et al., 2016) and reduce amphetamine-induced increases in extracellular DA concentrations (Bubser et al., 2014). Furthermore, fMRI studies showed that M_4 PAMs inhibit effects of amphetamine using cerebral blood volume (CBV) measurements in striatum and other forebrain structures (Byun et al., 2014). CBV fMRI is an indirect hemodynamic measure of neural activity. If M_4 PAMs inhibit D_1 signaling in the SNr by direct actions on D_1/cAMP signaling in D_1-SPNs, M_4 PAMs should inhibit effects of direct-acting D_1 agonists on CBV in this region. Injection of a behaviorally active dose of SKF82958 (1 mg/kg, i.p.) induced significant increases in CBV compared to baseline across the SNr, striatum as well as in the motor cortex (Figure 6A-D, Mann-Whitney test p<0.001 for each area). Interestingly, pre-treatment of rats with VU0467154 (30 mg/kg, i.p.) induced a significant reversal of SKF82958-induced increases in D_1 activation in the SNr, as well as the motor cortex, which is downstream of the SNr in the BG motor circuit (Figure 6A-B, D, Mann-Whitney test p<0.0001 for each area). These data are consistent with the hypothesis that M_4 activation inhibits D_1 signaling at the level of the SNr. Interestingly, in contrast to its effects on amphetamine-induced increases in CBV in the striatum (Byun et al., 2014), the M_4 PAM did not reverse the response to the D_1 agonist in the striatum (Figure 6A, C, Mann-Whitney test p>0.05). The finding that the M_4 PAM only reversed SKF82958-induced CBV responses in the SNr and motor cortex but not the striatum suggests that the M_4 PAM directly inhibits D_1 signaling in the SNr. Additionally, these data, combined with the previously reported ability of M_4 PAMs to inhibit striatal DA release and block CBV responses to amphetamine, suggest that M_4 PAM activity in the striatum may be more important in inhibiting responses to DA release (Bubser et al., 2014; Foster et al., 2016).

Interestingly, the M_4 PAM did not inhibit the CBV response to the D_1 agonist in regions that are not involved in regulation of motor function, including the sensory and cingulate cortices, or hippocampus (Figure 6A, E, Mann-Whitney test p>0.05). In contrast to its actions in the SNr, VU0467154 enhanced SKF82958-evoked changes in CBV in the hippocampus (Figure 6A, F, Wilcoxon-Mann-Whitney U test p<0.01) and induced a significant increase in the rise time of D_1 activation in the cingulate cortex as indicated by a faster rate of increase in CBV (Figure S6, Mann-Whitney test p<0.01). Additionally, we tested the effects of M_4 PAM administration alone to determine if we could detect baseline changes in CBV induced by the M_4 PAM, but did not observe any changes in any brain are examined (Figure S7 Mann-Whitney test p>0.05). This suggests that anesthesia during fMRI

may diminish brain responses and our signal to noise window to detect changes in BG output.

Local D_1 activation in the SNr is sufficient to increase locomotor activity and this effect is blocked by mAChR agonists

The present study raises the possibility that cholinergic projections and M_4 in the SNr may play a major role in regulating motor activity. To test this hypothesis, we performed a series of microinjection experiments to inject mAChR agonists or antagonists into the SNr. 15 minutes prior to microinjection, 3 mg/kg of the M_1 antagonist VU0255035 (i.p.) was given to block M_1 receptor activation (Xiang et al., 2012). We then unilaterally injected 1 μL of 0.5 mg/ml of Oxo-M or vehicle (sterile water) into the SNr. Oxo-M, but not vehicle, induced ipsilateral turning within the first 15 minutes after microinjection (Figure 7A, Mann-Whitney test p<0.01). Additionally, when the direct pathway was activated through systemic administration of 0.3 mg/kg SKF82958, microinjection of Oxo-M into the SNr produced rotations significantly different than baseline and not significantly different than the Oxo-M microinjection alone group (Figure 7A, Kruksal-Wallis, p<0.05). Microinjection of Oxo-M into the SNr of D_1-M_4 KO mice produces significantly fewer rotations than in littermate controls (Figure 7B, Mann-Whitney test, p<0.05) suggesting that activation of M_4 expressed on D_1-SPNs terminals in the SNr is sufficient to block locomotor activity.

Additionally, we microinjected 1 μL of 3 mg/ml scopolamine bi-laterally into the SNr to determine if antagonizing M_4 receptors in the SNr could alter locomotor activity. Consistent with our hypothesis, microinjection of scopolamine into the SNr increased locomotor activity of WT animals compared to vehicle (Figure 7C, One Way ANOVA with Tukey's Post Hoc test, p<0.05), but this effect was absent in D_1-M_4 KO mice (Figure 7C, One Way ANOVA with Tukey's Post Hoc test, p>0.05). While the volume of the microinjection likely caused spillover of scopolamine or Oxo-M into nearby brain regions, the absence of effect in D_1-M_4 KO animals suggests that the effect is mediated by M_4 in D_1-expressing SPNs. This provides *in vivo* evidence that inhibition of activity exerted by M_4 receptors on D_1-SPNs at the level of the SNr diminishes motor activity and removal of this inhibition increases locomotor activity.

Discussion

The striatum is critically involved in multiple brain functions, and is highly regulated by DA and ACh. DA inputs from the SNc regulate two separate populations of SPNs that give rise to the direct and indirect pathway projections (Albin et al., 1989; Alexander et al., 1990; Beaulieu and Gainetdinov, 2011). D_1-SPNs send inhibitory projections to the major output nuclei of the BG, including the SNr. Indirect pathway SPNs express D_2 DA receptors (D_2-SPNs), and have excitatory effects on SNr neurons by disinhibiting their major excitatory input (Albin et al., 1989; Beaulieu and Gainetdinov, 2011; Gerfen et al., 1990). The locomotor-stimulating effects of DA are primarily mediated by activation of D_1 and D_1-SPN projections to the SNr (Cabib et al., 1991; Wachtel et al., 1989). While activation of cholinergic pathways can have multiple effects on striatal function, a major role of mAChRs is to inhibit DA signaling and oppose D_1-mediated increases in locomotor activity (Foster et

al., 2014; Foster et al., 2016; Gomeza et al., 1999; Gomeza et al., 2001). This effect is thought to be mediated by release of ACh from ChIs projecting locally within the striatum (Aosaki et al., 1995; Aosaki et al., 2010; Bolam et al., 1984; Bonsi et al., 2011; Hersch et al., 1994; Wilson et al., 1990).

While most studies of cholinergic modulation of BG function have focused on ChIs in the striatum, recent studies suggest that cholinergic neurons of the PPN also project to the striatum and SNr (Beninato and Spencer, 1987; Butcher and Hodge, 1976; Saper and Loewy, 1982). The present study presents exciting new evidence that cholinergic projections from the PPN to the SNr activate M_4 in D_1-SPN terminals to directly inhibit D_1 signaling. This M_4-mediated response has a strong inhibitory influence on D_1-mediated increases in transmission at D_1-SPN synapses. The role of D_1 activation in increasing locomotor activity is well established (Beaulieu and Gainetdinov, 2011; Gerfen et al., 1990). The present study suggests that, in addition to striatal ChI activity, selective activation of M_4 in the SNr can strongly inhibit D_1 activation of D_1-SPN output and suppress related increases in locomotor activity.

Our studies are especially interesting in light of recent work demonstrating that optogenetic stimulation of cholinergic terminals from the PPN to DA neurons in the SNc induces depolarization of SNc DA neurons and increases locomotor activity (Xiao et al., 2015). Also, we recently reported that post-synaptic activation of mAChRs can depolarize SNr projection neurons (Xiang et al., 2012). Thus, PPN cholinergic projections are likely to have multiple actions on midbrain nuclei of the BG that are mediated by different ACh receptors and can have distinct actions to influence locomotor activity. This finding is directly analogous to the complex roles of ChIs on SPNs in the striatum, where selective M_4 activation reverses locomotor-stimulating effects of dopaminergic activation by inhibiting DA release (Foster et al., 2016), inhibiting D_1-responses in D_1-SPN cell bodies (Sánchez-Lemus and Arias-Montaño, 2006; Shen et al., 2015), inhibiting excitatory transmission, and promoting induction of long-term depression in D_1-SPNs (Pancani et al., 2015; Shen et al., 2015). However, activation of ChIs also induces depolarization of both D_1-SPNs and D_2-SPNs through activation of nAChRs (Benarroch, 2012) and M_1 (Xiang et al., 2012). Identifying individual ACh receptor subtypes involved in specific behaviors provides the opportunity to selectively modulate striatal function using receptor subtype-selective ligands.

The present findings are especially exciting in that they reveal that M_4 plays a powerful role in reducing DA signaling and regulation of locomotor activity at the level of the striatum and in D_1-SPN terminals in the SNr. Thus, one important implication of this study is the possibility that M_4-selective ligands may prove useful as novel therapeutic agents for treatment of disorders that involving dysregulation of dopaminergic signaling in the BG. Interestingly, mAChR antagonists were the first available treatments for PD (Vernier and Unna, 1956), and clinical studies demonstrate significant improvement in multiple aspects of motor function in patients receiving mAChR antagonists (Jankovic et al., 2007; Katzenschlager et al., 2003). However, non-selective mAChR antagonists have dose-limiting adverse effects that are likely mediated by blockade of M_1, M_2, and M_3 mAChRs (Drachman, 1977; Lang and Blair, 1989). The current study suggests that more robust efficacy and fewer adverse effects may be achieved with highly selective M_4 antagonists.

Additionally, our data indicate that M_4 induces a tonic inhibition of D_1-SPNs that is normally opposed by D_1 activity. This suggests that in DA-depleted states, tonic M_4-mediated inhibition of D_1-SPN activity is likely to predominate, and that this inhibition could be relieved by selective M_4 antagonists.

In addition to the potential clinical utility of M_4-selective antagonists, M_4 PAMs could be developed as treatments for disorders with excessive DA transmission. Consistent with this, M_4 PAMs have robust efficacy in multiple animal models of psychosis (Byun et al., 2014; Foster et al., 2016), HD (Pancani et al., 2015), addictive disorders (Dencker et al., 2012), and L-DOPA-induced dyskinesia (Shen et al., 2015). Importantly, selective actions of M_4 PAMs on DA transmission in the BG could provide a major advantage to the use of DA receptor antagonists, a mainstay for treatment of schizophrenia. While blockade of DA receptors in the BG can provide therapeutic benefits, blockade of DA receptors in the hippocampus and cortical regions can impair cognitive function (Lynch, 1992; Tsang et al., 2015; Yohn et al., 2015). Interestingly, our fMRI studies suggest that M_4 PAMs reduce CBV responses to D_1 agonists in the SNr and downstream motor cortex, but have no effect on responses to D_1 activation in cingulate cortex, hippocampus, and sensory cortex. In fact, the M_4 PAM enhanced responses to the D_1 agonist in hippocampus, and at early time points in the cingulate cortex. Based on this observation, and the mechanism by which M_4 PAMs locally inhibit DA release in the striatum (Foster et al., 2016), it is possible that M_4 PAMs can selectively reduce DA signaling in the BG without cognition-impairing or other adverse side effects of DA receptor antagonists. In agreement with this notion, recent studies suggest that M_4 PAMs enhance, rather than inhibit, hippocampal and cortical-dependent forms of cognitive function (Bubser et al., 2014; Grannan et al., 2014).

Taken together, our data support an expanded model of how DA and ACh can regulate D_1-SPNs (summarized in Figure 8), and suggest that regulation of D_1-SPN terminals in the SNr may play a more important role in regulating activity through the direct pathway than previously appreciated. Further understanding and testing the implications of this expanded model in terms of diseases of the BG is an exciting avenue for further investigation, may yield additional understanding of the circuitry of the BG, as well as open further novel therapeutic possibilities. Additionally, our data provide critical pre-clinical rationale and further understanding of the mechanistic underpinnings of the potential utility of M_4 antagonists or negative allosteric modulators for the treatment of movement disorders and M_4 PAMs for treatment of disorders that involve excessive DA transmission in the BG.

STAR Methods

CONTACT FOR REAGENT AND RESOURCE SHARING

Further information and requests for resources and reagents should be directed to and will be fulfilled by the Lead Contact, Dr. Jeff Conn (jeff.conn@vanderbilt.edu)

D_1-M_4 KO mice, and the mouse anti-M_4 antibodies are all subject to an MTA. Use of D_1-M_4 KO mice in this paper are governed by an MTA from Dr. Jurgen Wess at the NIDDK/NIH. M_4 antibodies are from the lab of Dr. Allen Levey at Emory University and are not

commercially available. VU0467154 used in this paper was made by the Vanderbilt University Center for Neuroscience Drug Discovery, but is also commercially available.

EXPERIMENTAL MODEL AND SUBJECT DETAILS

Animals: All *in vivo* and *ex vivo* experimental procedures were authorized by the Vanderbilt University Institutional Animal Care and Use Committee and conform to all NIH/PHS guidelines for use of animals in research.

D_1-M_4 KO mice (RRID: MGI:4442324; Jeon et al., 2010) were maintained through crosses of M_4(flox/flox) × M_4(flox/flox)/D_1-Cre animals. The D_1-Cre animal utilized for this were RRID:IMSR_JAX:030329. D_1-M_4 KO mice were maintained on a C57Bl6/J background, and this background was achieved from 10 backcrossings with C57Bl6/J mice prior to arriving at Vanderbilt University. Mice expressing ChR2/YFP selectively in ChAT-containing neurons (B6.Cg-Tg(Chat-COP4*H134R/EYFP, Slc18a3)5Gfng/J; RRID: IMSR_JAX014545) and mice that expressed the fluorescent reporter td-Tomato in D_1-expressing neurons (B6.Cg-Tg(Drd1a-tdTomato)6Calak/J; RRID: IMSR_JAX:016204) were maintained on C57Bl6/J backgrounds by crossings of an animal positive for the transgene with a wildtype animal. Wildtype animals, unless otherwise noted, are C57Bl6/J mice purchased from Jackson Laboratories (RRID: IMSR_JAX:000664). All animals used in these studies have a normal health and immune status. Male mice between 8 and 12 weeks of age were used for behavioral tests or 8 to 10 weeks for *ex vivo* studies, and animals were drug and test naïve at time of use. Mice were randomly assigned to experimental groups. Additionally, mice were maintained in AALAS approved vivariums on 12 hour light/dark cycles with *ad libitum* access to food and water. Mice were group housed except for mice that were used in microinjection experiments. Mice in these experiments were single housed after cannulation due to experimental concerns and health of the animal.

For phMRI studies, adult male Sprague-Daley rats between 250 and 275 g were purchased from Harlan (now Envigo). Rats were group housed until implanted with an IV catheter, and were single housed after cannulation. Rats were drug and test naïve at time of use, and were randomly assigned to experimental groups. The data analysts were blinded to dose group. Additionally, rats were maintained in AALAS approved vivariums on 12 hour light/dark cycles with *ad libitum* access to food and water.

METHOD DETAILS

Locomotor Testing—Locomotor activity was tested in wild-type and D_1-M_4 KO mice, 8–12 weeks old, using an open field system (OFA-510, MedAssociates, St. Albans, VT) with three 16×16 arrays of infrared photobeams. SKF82958-induced locomotor activity was assessed with the following paradigm: animals were habituated for 90 min in the open field before being injected with vehicle (10% tween-80 intraperitoneal (i.p.)) or VU0467154 (3, 10 or 30 mg/kg i.p., 10% tween-80 i.p.); 30 min later, vehicle (sterile water s.c.) or SKF82958 (1.0 mg/kg in sterile water subcutaneous (s.c.)) were administered, and locomotor activity was recorded for an additional 60 min (180 minute total session length). Data were analyzed using the activity software package (MedAssociates, St. Albans VT) and expressed as total beam breaks per 5 min bin.

Immunohistochemistry—D_1-td-Tomato mice were terminally anesthetized with an i.p. injection of ketamine (100 mg/kg) and xylazine (20mg/kg) cocktail and transcardially perfused with 0.1M PBS with 10 U/ml heparin and 2g/L glucose followed by ice-cold 4% paraformaldehyde (PFA) made in 0.1M PBS. Brains were dissected and postfixed at 4°C for 2 hours in 4% PFA, and then transferred to 30% sucrose in PBS at 4°C for cryopreservation. Once brains were saturated in sucrose, they were flash-frozen in a −55°C 2-methylbutane dry-ice bath and stored at −80°C until sectioning. Brains were sectioned at 40 μm on a sledge microtome (Leica, Deerfield, IL).

After sectioning, brain slices were stored at −20°C in 50% glycerol in 0.1M PBS. Sections were rinsed three times with PBS. Sections were blocked by incubating sections for 1 hour in 5% normal donkey serum 5% normal horse serum containing 0.1% Triton X-100 in PBS at 4°C with agitation. After initial blocking, sections were stained using the mouse-on-mouse (M.o.M) primary antibody kit (Vector Labs, Berlingame, CA) modified for use with fluorescent secondary. Following three rinses in PBS, sections were incubated in M.o.M mouse IgG blocking buffer for 1 hour at room temperature, then washed 2 times in PBS. Sections were then incubated in M.o.M kit diluent and sections were then transferred to 1:100 mouse anti-M4 (see Levey et al 1991) in kit diluent for 24 hours at 4°C. After incubation in primary antibodies, sections were washed three times in PBS. Sections were then incubated in secondary antibodies diluted in kit diluent with 1:500 donkey anti mouse IgG conjugated with Alexa-647(Jackson Immuno-Research, West Grove, PA) for 2 hours at room temperature, and then washed 3 times in PBS. Sections were then mounted to positively charged glass slides (ThermoFisher, New York, NY), air-dried, and mounted in pro-long gold mounting media (Life Technologies, Grand Island, NY). Slides were imaged on a Zeiss LSM 510 inverted confocal. During imaging, Alexa-647 was false colored to green in order to aid in visualization of co-localization of signal with td-tomato.

Stereotaxic Surgeries—Mice were anesthetized using continuous isoflurane anesthesia at 5%, 2 L/min and anesthesia was maintained at 1-2%, 2L/min during surgery. All surgeries were performed using a Kopf digital stereotaxic frame (Kopf, Hercules, CA). For stereotaxic viral injections of the Opto-XR and hM4Di DREADD (both from UNC Viral Vector Core), virus was infused over 10 min at 0.15 μl/min into the striatum via a gastight syringe fitted with a 31 g needle (Hamiliton, Reno, NV) placed at the following coordinates (in mm): AP: +0.8; ML: −1.8; DV: −2.3. For retrobead injections into the SNr, injections were performed at at: AP:−4.35; ML: ±1.1; DV: −3.5. For viral injections into the PPN, injections were performed at at: AP:−4.35; ML: ±1.1; DV: −3.5.. For cannula implantation for rotational behaviors, a 26 g cannula was implanted at: AP:−3.28; ML: ±1.37; DV: −4.5. To verify placement, dye was injected down the cannula, the brain rapidly removed, and the brain sectioned with the aid of a brain matrix. Dye location was compared to a brain atlas to estimate location of cannula placement. Cannula placement was verified by an experimenter who did not perform the surgeries or behavioral experiments. All coordinates are relative to bregma and the dural surface.

Whole-Cell Patch Clamp Electrophysiology—Mice were anesthetized by i.p. injection of a solution composed of ketamine (100 mg/kg) and xylazine (20 mg/kg) and then

transcardially perfused with cold, sucrose-modified artificial cerebrospinal fluid (sACSF, in mM; 210 sucrose, 2.5 KCl, 8 $MgSO_4$, 0.5 $CaCl_2$, 1.25 NaH_2PO_4, 26 $NaHCO_3$, and 10 D-glucose). Mice were then decapitated and the brains were removed. 300 μm coronal sections of the SNr were made on a Compresstome VF-700 (Precisionary Instruments, San Jose, CA). After sectioning, coronal slices were submerged for 10–15 min at 32 °C in protective media containing 92 mM *N*-methyl-D-glucamine (NMDG), 2.5 mM KCl, 1.2 mM NaH_2PO_4, 30 mM $NaHCO_3$, 20 mM Hepes, 25 mM D-glucose, 5 mM sodium ascorbate, 2 mM thiourea, 3 mM sodium pyruvate, 10 mM $MgSO_4$, 0.5 mM $CaCl_2$ (pH 7.3) at 295-300 mOsm. Following this recovery period, slices were transferred to ACSF containing 126 mM NaCl, 2.5 mM KCl, 26.2 mM $NaHCO_3$, 1.25 mM NaH_2PO_4, 2 mM $CaCl_2$, 1.5 mM $MgSO_4$, 10 mM D-glucose and 5 mM sodium ascorbate.

Whole cell voltage-clamp signal was amplified using Axon Multiclamp 700B amplifiers (Molecular Devices, Sunnyvale, CA) with appropriate electrode-capacitance compensation and bridge balance. Patch pipets were prepared from borosilicate glass (Sutter Instrument Company) using a P-97 Flaming/Brown micropipet puller (Sutter Instruments), and had resistance of 3–6 MΩ when filled with the following intracellular solution (mM): 130 CsCl, 10 NaCl, 0.25 $CaCl_2$, 2 $MgCl_2$, 5 EGTA, 10 HEPES, 10 glucose, 2 Mg-ATP. The pH of the pipet solution was adjusted to 7.3 with 1 M CsOH, and osmolarity was adjusted to 285–290. Whole cell recordings were made from visually identified cells in the SNr under an Olympus BX50WI upright microscope (Olympus, Lake Success, NY). A low-power objective (4×) was used to identify the SNr, and a 40× water immersion objective coupled with Hoffman optics was used to visualize the individual neurons. GABAergic cells of the SNr were identified by previously determined membrane characteristics and firing rates (Radnikow and Misgeld, 1998).

To isolate mIPSCs, slices were superfused continuously at a rate of ~2.0 ml/min with an oxygenated solution containing (in mM): 126 mM NaCl, 2.5 mM KCl, 26.2 mM $NaHCO_3$, 1.25 mM NaH_2PO_4, 2 mM $CaCl_2$, 1.5 mM $MgSO_4$, 10 mM D-glucose, pH 7.35 with 0.5 μM tetrodotoxin (TTX, Abcam, Cambridge, UK), 5 μM AMPA receptor 6-cyano-7-nitroquinoxaline-2,3-dione (CNQX, Tocris, Bristol, UK) and 1 μM NMDA receptor antagonist DL-2-amino-4-methyl-5-phosphono-3-pentenoic acid (AP-4) (Sigma, St. Louis, MO). Slices were perfused with this solution at 25 °C for at least 15 minutes following establishment of electrical access. Access resistances were <15 MΩ. mIPSCs were recorded from GABAergic cells of the SNr held at −70 mV in GAP free mode. Time course of experiments were as follows: after 5 min of stable baseline recordings, SKF89258 or forskolin were bath applied to slices for 5 min, then washout for another 5 minutes. For block experiments, the time course was: after 5 min of stable baseline recordings, muscarinic agents were pre-applied for 5 minutes, then muscarinic agents were co-applied with SKF89258 or forskolin for 5 min, then washout for another 5 minutes. All drugs were bath-applied with the complete exchange of the external solution not exceeding 30 sec. Data were acquired using Digidata 1440A and pClamp 9.2 and analyzed with Mini Analysis software (Synaptosoft).

For optogenetic stimulation with the ChAT- ChR2 constructs, we used a CoolLED pE-100 illumination system (CoolLED, Brighton, U.K.) under the control of a pulser (Prizmatix,

Givat-Schmuel, Israel) connected to the Olympus microscope. The 473 nm blue light beam was applied to the slice through the 40× water immersion objective. For ChAT-ChR2 experiments, 10 Hz 5ms pulses at 22 mW were given. For ChAT-ChR2 experiments, the addition of DhβE (1μM) and mecamylamine (5 μM) was added to the ACSF in addition to TTX, CNQX and AP-5 to block currents associated with nAChRs. For Opto XR experiments 500 ms continuous pulses were given at 10 mW. Slice preparation and recording conditions were as above.

Pharmacological Magnetic Resonance Imaging (phMRI)—Contrast-enhanced cerebral blood volume (CBV) fMRI was used as an indirect hemodynamic measure of drug-induced changes in brain activity *in vivo* (Byun et al, 2014) Isoflurane-anesthetized rats with preimplanted jugular vein catheters underwent endotracheal intubation (14 G catheter), insertion of i.p. and s.c. catheters (size P50; Braintree Scientific, Braintree, MA), and mechanical ventilation (Kent Scientific, Litchfield, CT; $O_2:N_2O$ 1 : 2; 2% isoflurane). For scanning, isoflurane was set to 0.9% and neuromuscular blocker was administered (vecuronium bromide, 1 mg/kg, i.p.). Pulse rate, respiration, and rectal temperature were continuously monitored (transimaging.com Raleigh, NC) and temperature maintained through an air-heating unit (SAM-PC; SA Instruments, Encinitas, CA). End-tidal CO_2 was continuously monitored (Invivo Research, Orlando, FL). PhMRI data were acquired using a 9.4T Varian magnet controlled by a Varian Inova console (Agilent, Palo Alto, CA) with a with a Doty litz 38-mm transmit-receive radiofrequency coil. High-resolution fast spin-echo (fse) structural images were collected (repetition time [TR] 2550 ms; effective echo time [TEeff] 40 ms; number of excitations [NEX] 2; 128 × 128 matrix; 35 × 35 mm2 field of view; 14 contiguous slices, 1.0 mm thick). Pre-contrast reference images and post-contrast functional images were acquired (fse: TR 2600 ms; TEeff 36 ms; NEX 2; 64 × 64 matrix). To measure cerebral CBV, Molday iron oxide nanoparticles (MION, 30 nm; 20 mg/kg, i.v.; BioPAL, Worcester, MA) were injected and allowed to equilibrate. A 5-minute baseline was collected, then all subjects were administered vehicle or 30 mg/kg VU0467154 (i.p.) After 30 min, all rats were administered SKF89258 during the continuous data acquisition.

PhMRI data were processed using in-house MATLAB code (MathWorks, Natick, MA) and Analysis of Functional NeuroImages (AFNI; afni.nimh.nih.gov). All brain-masked, motion-corrected (AFNI 2dreg) images were coregistered to the template anatomical images in AFNI. Fractional CBV changes were calculated on a voxel-wise basis for each subject using the equation: $CBV(t)/CBVo = [\ln S(t) - \ln So]/[\ln So - \ln Spre]$, where $S(t)$ is the measured signal at time t, So is the post-contrast baseline signal, and Spre is the pre-contrast baseline. Regions of interest (ROIs), pre-defined on the template, based on a rat brain atlas (Paxinos and Watson, 2007), were applied to all coregistered subjects. Mean CBV changes (left and right hemispheres averaged) were calculated for each region of interest. Mean CBV changes were groups were compared between the two treatment groups using the Mann Whitney test in GraphPad Prism V5.04 (GraphPad Software, La Jolla, CA).

<u>Rotation Behavioral Assay:</u> After cannula implantation as described above, mice were allowed to recover, singly housed for 1 week. 15 minutes prior to the testing session, animals were given 3 mg/kg in 10% Tween-80 of the M_1 antagonist VU0255035 to prevent seizure-

like activity. Vehicle (10% Tween 80) or 0.3 mg/kg SKF89258 i.p were also injected 15 minutes prior to microinjection. A 30 gauge needle was then placed through the guide cannula and 1 μL of 0.5 mg/mL Oxo-M or 1 μL of sterile water was microinjected into the SNr. Mice were placed into a cylinder and recorded for 15 min. A reviewer blinded to experimental conditions then scored the videos for total contralateral rotations.

Bilateral Microinjection Assay: After bi-lateral cannula implantation as described above, mice were allowed to recover, singly housed for 1 week. WT littermates or D_1-M_4 KO animals were placed in an open field system (OFA-510, MedAssociates, St. Albans, VT) with three 16×16 arrays of infrared photobeams for 90 min to habituate before being bilaterally microinjected with 1 μL vehicle (sterile water) or scopolamine (3mg/ml); and locomotor activity was recorded for an additional 60 min. Data were analyzed using the activity software package (MedAssociates, St. Albans VT) and for the 60 minutes following microinjection expressed as total distance travelled.

QUANTIFICATION AND STATISTICAL ANALYSIS

All statistical analyses were performed in GraphPad Prism 5 (GraphPad, San Diego, CA). Various statistical tests were used throughout the paper with the following rationale: If the data were normally distributed as determined by a D'Agonstino and Pearson omnibus normality test, a t-test (one or two tailed, or comparing to a hypothetical mean) was used for tests comparing 2 conditions. A one way ANOVA was utilized with either a Tukey's or Dunnett's post-hoc comparison were used for data that had 3 or more conditions. If the data were not normally distributed a Wilcoxon matched pairs and rank test was used if there were two conditions and Kruksal-Wallis test with Dunnett's post comparison was used. All data in this paper are represented as mean with standard error of the mean. N, which represents individual animals in behavioral tests and individual cells in electrophysiology experiments, can be found in each figure legend.

Supplementary Material

Refer to Web version on PubMed Central for supplementary material.

Acknowledgments

References

Albin RL, Young AB, Penney JB. The functional anatomy of basal ganglia disorders. Trends Neuorscience. 1989; 12:366–375.

Alexander GE, Crutcher MD, DeLong MR. Basal ganglia-thalamocortical circuits: parallel substrates for motor, oculomotor, prefrontal and limbic functions. Prog Brain Res. 1990; 85:119–146. [PubMed: 2094891]

Aosaki T, Kimura M, Graybiel AM. Temporal and spatial characteristics of tonically active neurons of the primate's striatum. J Neurophysiol. 1995; 73:1234–1252. [PubMed: 7608768]

Aosaki T, Miura M, Suzuki T, Nishimura K, Masuda M. Acetylcholine–dopamine balance hypothesis in the striatum: An update. Geriatr Gerontology Int. 2010; 10:S148–S157.

Beaulieu JM, Gainetdinov RR. The physiology, signaling, and pharmacology of dopamine receptors. Phamacol Rev. 2011; 63:182–217.

Benarroch EE. Effects of acetylcholine in the striatum Recent insights and therapeutic implications. Neurology. 2012; 79:274–281. [PubMed: 22802594]

Bendor J, Lizardi-Ortiz JE, Westphalen RI, Brandstetter M, Hemmings HC, Sulzer D, Flajolet M, Greengard P. AGAP1/AP-3-dependent endocytic recycling of M(5) muscarinic receptors promotes dopamine release. EMBO J. 2010; 29:2813–2826. [PubMed: 20664521]

Beninato M, Spencer RF. A cholinergic projection to the rat substantia nigra from the pedunculopontine tegmental nucleus. Braine Res. 1987; 412:169–174.

Bolam JP, Wainer BH, Smith AD. Characterization of cholinergic neurons in the rat neostriatum. A combination of choline acetyltransferase immunocytochemistry, Golgi-impregnation and electron microscopy. Neurosci. 1984; 12:711–718.

Bonsi P, Cuomo D, Martella G, Madeo G, Schirinzi T, Puglisi F, Ponterio G, Pisani A. Centrality of Striatal Cholinergic Transmission in Basal Ganglia Function. Front Neuroanat. 2011; 5:6. [PubMed: 21344017]

Borgkvist A, Avegno EM, Wong MY, Kheirbek MA, Sonders MS, Hen R, Sulzer D. Loss of Striatonigral GABAergic Presynaptic Inhibition Enables Motor Sensitization in Parkinsonian Mice. Neuron. 2015; 87:976–988. [PubMed: 26335644]

Brady AE, Jones CK, Bridges TM, Kennedy JP, Thompson AD, Heiman JU, Breininger ML, Gentry PR, Yin H, Jadhav SB, et al. Centrally Active Allosteric Potentiators of the M(4) Muscarinic Acetylcholine Receptor Reverse Amphetamine-Induced Hyperlocomotor Activity in Rats. J Pharmacol Exp Ther. 2008; 327:941–953. [PubMed: 18772318]

Bubser M, Bridges TM, Dencker D, Gould RW, Grannan M, Noetzel MJ, Lamsal A, Niswender CM, Daniels JS, Poslusney MS, et al. Selective Activation of M4 Muscarinic Acetylcholine Receptors Reverses MK-801-Induced Behavioral Impairments and Enhances Associative Learning in Rodents. ACS Chem Neuroci. 2014; 5:920–942.

Butcher LL, Hodge GK. Postnatal development of acetylcholinesterase in the caudate-putamen nucleus and substantia nigra of rats. Brain Res. 1976; 106:223–240. [PubMed: 1276870]

Byun NE, Grannan M, Bubser M, Barry RL, Thompson A, Rosanelli J, Gowrishankar R, Kelm ND, Damon S, Bridges TM, et al. Antipsychotic drug-like effects of the selective M4 muscarinic acetylcholine receptor positive allosteric modulator VU0152100. Neuropsychopharmacol. 2014; 39:1578–1593.

Cabib S, Castellano C, Cestari V, Filibeck U, Puglisi-Allegra S. D1 and D2 receptor antagonists differently affect cocaine-induced locomotor hyperactivity in the mouse. Psychopharmacol. 1991; 105:335–339.

Cachope R, Cheer JF. Local control of striatal dopamine release. Front Behav Neurosci. 2014; 8:188. [PubMed: 24904339]

Conn PJ, Jones CK, Lindsley CW. Subtype-selective allosteric modulators of muscarinic receptors for the treatment of CNS disorders. Trends Pharmacol Sci. 2009; 30:148–155. [PubMed: 19201489]

Corvol JC, Valjent E, Pascoli V, Robin A, Stipanovich A, Luedtke RR, Belluscio L, Girault JA, Herve D. Quantitative changes in Galphaolf protein levels, but not D1 receptor, alter specifically acute responses to psychostimulants. Neuropsychopharmacol. 2007; 32:1109–1121.

Crunelle CL, Miller ML, Booij J, van den Brink W. The nicotinic acetylcholine receptor partial agonist varenicline and the treatment of drug dependence: A review. Eur Neuropsychopharmacol. 2010; 20:69–79. [PubMed: 19959340]

Dautan D, Huerta-Ocampo I, Witten IB, Deisseroth K, Bolam JP, Gerdjikov T, Mena-Segovia J. A major external source of cholinergic innervation of the striatum and nucleus accumbens originates in the brainstem. J Neurosci. 2014; 34:4509–4518. [PubMed: 24671996]

Dencker D, Weikop P, Sørensen G, Woldbye DPD, Wörtwein G, Wess J, Fink-Jensen A. An allosteric enhancer of M(4) muscarinic acetylcholine receptor function inhibits behavioral and neurochemical effects of cocaine. Psychopharmacol. 2012; 224:277–287.

Drachman DA. Memory and cognitive function in man: does the cholinergic system have a specific role? Neurology. 1977; 27:783–790. [PubMed: 560649]

Drago J, Padungchaichot P, Wong JYF, Lawrence AJ, McManus JF, Sumarsono SH, Natoli AL, Lakso M, Wreford N, Westphal H, et al. Targeted Expression of a Toxin Gene to D1 Dopamine Receptor Neurons by Cre-Mediated Site-Specific Recombination. J Neurosci. 1998; 18:9845–9857. [PubMed: 9822743]

Foster DJ, Gentry PR, Lizardi-Ortiz JE, Bridges TM, Wood MR, Niswender CM, Sulzer D, Lindsley CW, Xiang Z, Conn PJ. M5 receptor activation produces opposing physiological outcomes in dopamine neurons depending on the receptor's location. J Neurosci. 2014; 34:3253–3262. [PubMed: 24573284]

Foster DJ, Wilson JM, Remke DH, Mahmood MS, Uddin MJ, Wess J, Patel S, Marnett LJ, Niswender CM, Jones CK, et al. Antipsychotic-like Effects of M4 Positive Allosteric Modulators Are Mediated by CB2 Receptor-Dependent Inhibition of Dopamine Release. Neuron. 2016; 91:1244–1252. [PubMed: 27618677]

Gerfen CR, Engber TM, Mahan LC, Susel Z, Chase TN, Monsma FJ Jr, Sibley DR. D1 and D2 dopamine receptor-regulated gene expression of striatonigral and striatopallidal neurons. SCIENCE (New York, NY). 1990; 250:1429–1432.

Gomeza J, Zhang L, Kostenis E, Felder C, Bymaster F, Brodkin J, Shannon H, Xia B, Deng C-x, Wess J. Enhancement of D1 dopamine receptor-mediated locomotor stimulation in M(4) muscarinic acetylcholine receptor knockout mice. P Natl Acad Sci. 1999; 96:10483–10488.

Gomeza J, Zhang L, Kostenis E, Felder CC, Bymaster FP, Brodkin J, Shannon H, Xia B, Duttaroy A, Deng C-x, et al. Generation and pharmacological analysis of M2 and M4 muscarinic receptor knockout mice. Life Sci. 2001; 68:2457–2466. [PubMed: 11392613]

Goodchild RE, Grundmann K, Pisani A. New genetic insights highlight 'old' ideas on motor dysfunction in dystonia. Trends Neurosci. 2013; 36:717–725. [PubMed: 24144882]

Grannan M, Bubser M, Bridges T, Gould R, Dencker Thorbek D, Daniels J, Noetzel M, Niswender C, Duggan M, Brandon N, et al. Effects of the M4 muscarinic receptor positive allosteric modulator VU0467154 on cognition and pyramidal cell firing properties in layer V of the mPFC. FASEB. 2014; 28

Graybiel AM. Habits, rituals, and the evaluative brain. Ann Rev Neurosci. 2008; 31:359–387. [PubMed: 18558860]

Guo ML, Fibuch EE, Liu XY, Choe ES, Buch S, Mao LM, Wang JQ. CaMKIIα interacts with M4 muscarinic receptors to control receptor and psychomotor function. EMBO. 2010; 29:2070–2081.

Hersch SM, Gutekunst CA, Rees HD, Heilman CJ, Levey AI. Distribution of m1-m4 muscarinic receptor proteins in the rat striatum: light and electron microscopic immunocytochemistry using subtype-specific antibodies. J Neurosci. 1994; 14:3351–3363. [PubMed: 8182478]

Herve D. Identification of a specific assembly of the g protein golf as a critical and regulated module of dopamine and adenosine-activated cAMP pathways in the striatum. Front Neuroanat. 2011; 5:48. [PubMed: 21886607]

Holt DJ, Herman MM, Hyde TM, Kleinman JE, Sinton CM, German DC, Hersh LB, Graybiel AM, Saper CB. Evidence for a deficit in cholinergic interneurons in the striatum in schizophrenia. Neurosci. 1999; 94:21–31.

Jankovic J, Watts RL, Martin W, Boroojerdi B. Transdermal rotigotine: double-blind, placebo-controlled trial in Parkinson disease. Arch Neurol. 2007; 64:676–682. [PubMed: 17502466]

Jeon J, Dencker D, Wortwein G, Woldbye DPD, Cui Y, Davis AA, Levey AI, Schütz G, Sager T, Mørk A, et al. A Subpopulation of Neuronal M(4) Muscarinic Acetylcholine Receptors Plays a Critical Role in Modulating Dopamine-Dependent Behaviors. J Neurosci. 2010; 30:2396–2405. [PubMed: 20147565]

Kataoka Y, Kalanithi PS, Grantz H, Schwartz ML, Saper C, Leckman JF, Vaccarino FM. Decreased number of parvalbumin and cholinergic interneurons in the striatum of individuals with Tourette syndrome. J Comp Neurol. 2010; 518:277–291. [PubMed: 19941350]

Katz LC, Burkhalter A, Dreyer WJ. Fluorescent latex microspheres as a retrograde neuronal marker for in vivo and in vitro studies of visual cortex. Nature. 1984; 310:498–500. [PubMed: 6205278]

Katzenschlager R, Sampaio C, Costa J, Lees A. Anticholinergics for symptomatic management of Parkinson's disease. Cochrane Db System Rev. 2003:Cd003735.

Krashes MJ, Koda S, Ye C, Rogan SC, Adams AC, Cusher DS, Maratos-Flier E, Roth BL, Lowell BB. Rapid, reversible activation of AgRP neurons drives feeding behavior in mice. J Clin Invest. 2011; 121:1424–1428. [PubMed: 21364278]

Kruse AC, Kobilka BK, Gautam D, Sexton PM, Christopoulos A, Wess J. Muscarinic acetylcholine receptors: novel opportunities for drug development. Nat Rev Drug Discov. 2014; 13:549–560. [PubMed: 24903776]

Lang, AE., Blair, RDG. Anticholinergic Drugs and Amantadine in the Treatment of Parkinson's Disease. In: Calne, DB., editor. Drugs for the Treatment of Parkinson's Disease. Berlin, Heidelberg: Springer Berlin Heidelberg; 1989. p. 307-323.

Levey AI, Kitt CA, Simonds WF, Price DL, Brann MR. Identification and localization of muscarinic acetylcholine receptor proteins in brain with subtype-specific antibodies. J Neurosci. 1991; 11:3218–3226. [PubMed: 1941081]

Lynch MR. Schizophrenia and the D1 receptor: focus on negative symptoms. Prog Neuropshychopharm. 1992; 16:797–832.

Onali P, Olianas MC. Muscarinic M4 receptor inhibition of dopamine D1-like receptor signalling in rat nucleus accumbens. Eur J Pharmacol. 2002; 448:105–111. [PubMed: 12144929]

Pancani T, Foster DJ, Moehle MS, Bichell TJ, Bradley E, Bridges TM, Klar R, Poslusney M, Rook JM, Daniels JS, et al. Allosteric activation of M4 muscarinic receptors improve behavioral and physiological alterations in early symptomatic YAC128 mice. P Natl Acad Sci. 2015; 112:14078–14083.

Picciotto, Marina R., Higley, Michael J., Mineur, Yann S. Acetylcholine as a Neuromodulator: Cholinergic Signaling Shapes Nervous System Function and Behavior. Neuron. 2012; 76:116–129. [PubMed: 23040810]

Pisani A, Bernardi G, Ding J, Surmeier DJ. Re-emergence of striatal cholinergic interneurons in movement disorders. Trends Neurosci. 2007; 30:545–553. [PubMed: 17904652]

Pisani A, Centonze D, Bernardi G, Calabresi P. Striatal synaptic plasticity: implications for motor learning and Parkinson's disease. Mov Disord. 2005; 20:395–402. [PubMed: 15719415]

Radnikow G, Misgeld U. Dopamine D1 receptors facilitate GABAA synaptic currents in the rat substantia nigra pars reticulata. J Neurosci. 1998; 18:2009–2016. [PubMed: 9482788]

Sánchez-Lemus E, Arias-Montaño JA. M1 muscarinic receptors contribute to, whereas M4 receptors inhibit, dopamine D1 receptor-induced [3H]-cyclic AMP accumulation in rat striatal slices. Neurochem Res. 2006; 31:555–561. [PubMed: 16758365]

Saper CB, Loewy AD. Projections of the pedunculopontine tegmental nucleus in the rat: evidence for additional extrapyramidal circuitry. BRAIN RES. 1982; 252:367–372. [PubMed: 7150958]

Shen W, Plotkin JL, Francardo V, Ko WK, Xie Z, Li Q, Fieblinger T, Wess J, Neubig RR, Lindsley CW, et al. M4 Muscarinic Receptor Signaling Ameliorates Striatal Plasticity Deficits in Models of L-DOPA-Induced Dyskinesia. Neuron. 2015; 88:762–773. [PubMed: 26590347]

Shin JH, Adrover MF, Wess J, Alvarez VA. Muscarinic regulation of dopamine and glutamate transmission in the nucleus accumbens. P Natl Acad Sci. 2015; 112:8124–8129.

Silberberg G, Bolam JP. Local and afferent synaptic pathways in the striatal microcircuitry. Curr Opin Neurobiol. 2015; 33:182–187. [PubMed: 26051382]

Siuda ER, McCall JG. Optodynamic simulation of beta-adrenergic receptor signalling. Nat Commun. 2015; 6:8480. [PubMed: 26412387]

Starke K, Gothert M, Kilbinger H. Modulation of neurotransmitter release by presynaptic autoreceptors. Physiol Rev. 1989; 69:864–989. [PubMed: 2568648]

Tanimura A, Pancani T, Lim SAO, Tubert C, Melendez AE, Shen W, Surmeier DJ. Striatal cholinergic interneurons and Parkinson's disease. Eur J Neurosci. 2017; doi: 10.1111/ejn.13638

Trevitt JT, Carlson BB, Nowend K, Salamone JD. Substantia nigra pars reticulata is a highly potent site of action for the behavioral effects of the D1 antagonist SCH 23390 in the rat. Psychopharmacol. 2001; 156:32–41.

Trevitt T, Carlson B, Correa M, Keene A, Morales M, Salamone JD. Interactions between dopamine D1 receptors and gamma-aminobutyric acid mechanisms in substantia nigra pars reticulata of the rat: neurochemical and behavioral studies. Psychopharmacol. 2002; 159:229–237.

Tsang J, Fullard JF, Giakoumaki SG, Katsel P, Katsel P, Karagiorga VE, Greenwood TA, Braff DL, Siever LJ, Bitsios P, et al. The relationship between dopamine receptor D1 and cognitive performance. NPJ Schiz. 2015; 1:14002.

Vernier VG, Unna KR. The experimental evaluation of antiparkinsonian compounds. Ann NY Acad Sci. 1956; 64:690–704. [PubMed: 13373238]

Wachtel SR, Hu XT, Galloway MP, White FJ. D1 dopamine receptor stimulation enables the postsynaptic, but not autoreceptor, effects of D2 dopamine agonists in nigrostriatal and mesoaccumbens dopamine systems. Synapse. 1989; 4:327–346. [PubMed: 2532422]

Wen P, Li M, Xiao H, Ding R, Chen H, Chang J, Zhou M, Yang Y, Wang J, Zheng W, et al. Low-frequency stimulation of the pedunculopontine nucleus affects gait and the neurotransmitter level in the ventrolateral thalamic nucleus in 6-OHDA Parkinsonian rats. Neurosci Lett. 2015; 600:62–68. [PubMed: 26054938]

Wichmann T, DeLong MR. Functional and pathophysiological models of the basal ganglia. Curr Opin Neurobio. 1996; 6:751–758.

Wilson CJ, Chang HT, Kitai ST. Firing patterns and synaptic potentials of identified giant aspiny interneurons in the rat neostriatum. J Neurosci. 1990; 10:508–519. [PubMed: 2303856]

Xiang Z, Thompson AD, Jones CK, Lindsley CW, Conn PJ. Roles of the M1 Muscarinic Acetylcholine Receptor Subtype in the Regulation of Basal Ganglia Function and Implications for the Treatment of Parkinson's Disease. J Pharmacol Exp Ther. 2012; 340:595–603. [PubMed: 22135383]

Xiao C, Cho Jounhong R, Zhou C, Treweek Jennifer B, Chan K, McKinney Sheri L, Yang B, Gradinaru V. Cholinergic Mesopontine Signals Govern Locomotion and Reward through Dissociable Midbrain Pathways. Neuron. 2015; 90:333–347.

Yang CF, Chiang M, Gray DC, Prabhakaran M, Alvarado M, Juntti SA, Unger EK, Wells JA, Shah NM. Sexually dimorphic neurons in the ventromedial hypothalamus govern mating in both sexes and aggression in males. Cell. 2013; 153:896–909. [PubMed: 23663785]

Yohn SE, Santerre JL, Nunes EJ, Kozak R, Podurgiel SJ, Correa M, Salamone JD. The role of dopamine D1 receptor transmission in effort-related choice behavior: Effects of D1 agonists. Pharmacol Biochem Be. 2015; 135:217–226.

Zhang W, Yamada M, Gomeza J, Basile AS, Wess J. Multiple muscarinic acetylcholine receptor subtypes modulate striatal dopamine release, as studied with M1-M5 muscarinic receptor knock-out mice. J Neurosci. 2002; 22:6347–6352. [PubMed: 12151512]

Zhuang X, Belluscio L, Hen R. G(olf)alpha mediates dopamine D1 receptor signaling. J Neurosci. 2000; 20:Rc91. [PubMed: 10924528]

Highlights

1. M_4 activation can inhibit D_1 dopamine receptor signaling.

2. The site of action for this novel mechanism is in the SNr and not in the striatum.

3. M_4 signaling may tonically inhibit the BG direct pathway

4. Hindbrain sources of acetylcholine are capable of regulating the BG direct pathway.
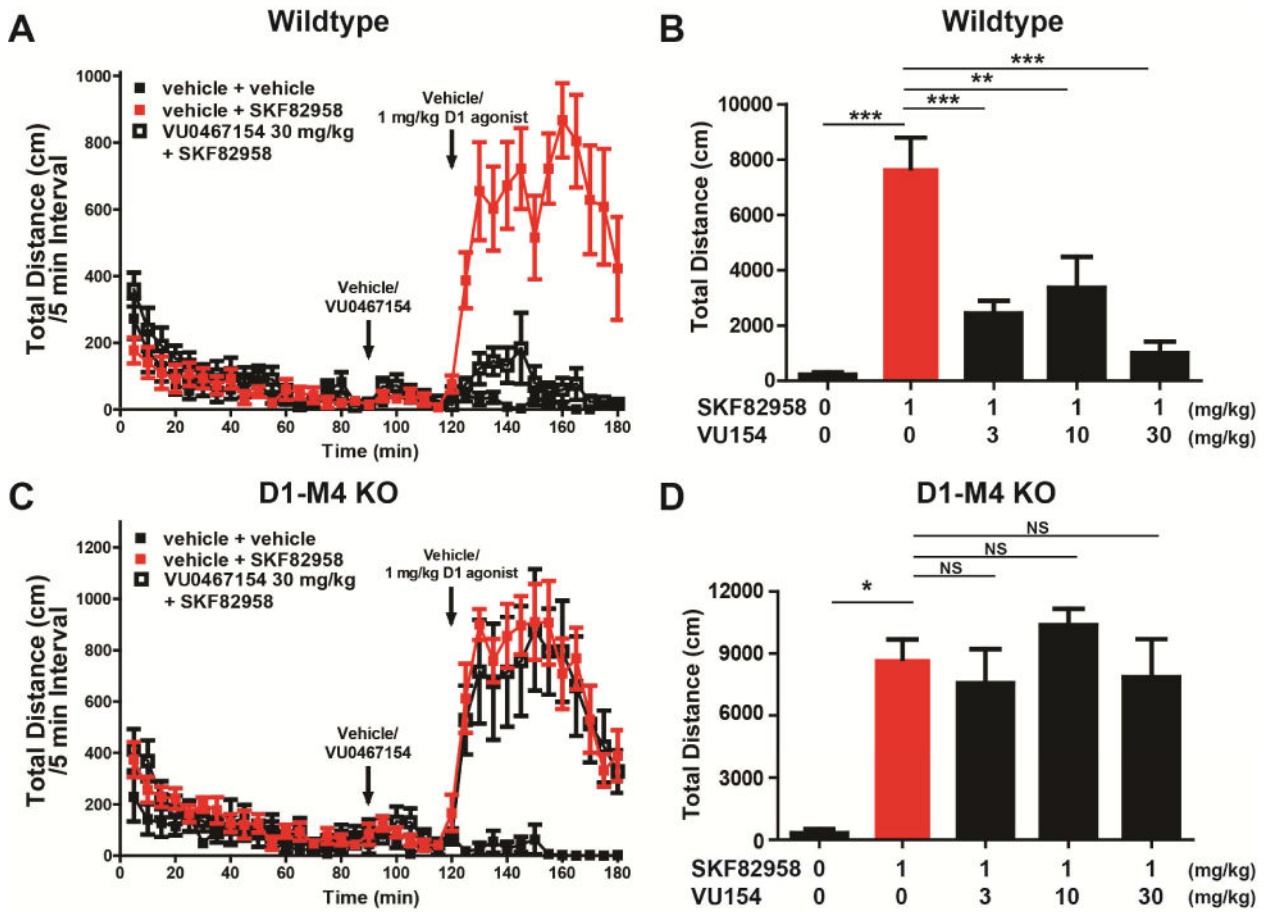
Figure 1. D₁ agonists increase locomotion and is reversed by administration of the M₄ PAM, VU0467154

A) WT animals were injected with M₄ PAM VU0467154 (30 mg/kg, intraperitoneal (i.p.), 10% Tween 80) 90 minutes after being placed in locomotion chambers. Thirty minutes later, D₁ agonist SKF82958 was administered (1 mg/kg, i.p., sterile water). Activity was then recorded for an additional 60 min and reported as distance in centimeters (cm) per 5 minute bins. **B)** Dose-response relationship of 3, 10, and 30 mg/kg VU0467154 (i.p., 10% Tween 80) in WT mice following the injection pattern in **(A)**. Data are the total distance moved in cm after the injection of amphetamine,. **C)** D₁-M₄ KO mice were injected with M₄ PAM VU0467154, SKF82958, and/or veh as in **(A)**. **D)** Dose- response relationship of 3, 10, and 30 mg/kg VU0467154 (i.p., 10% Tween 80) in D₁-M₄ KO mice following the same pattern in **(A)**. VU0467154 is unable to block D₁-induced hyper locomotion in D₁-M₄ KO mice. See also Figure S1. Data are mean ± SEM with an n=8-12 per treatment group. * indicates p<0.05, ** indicates p<0.01, *** indicates p<0.001, NS indicates not statistically significant by one way ANOVA followed by Tukey's post-hoc test.
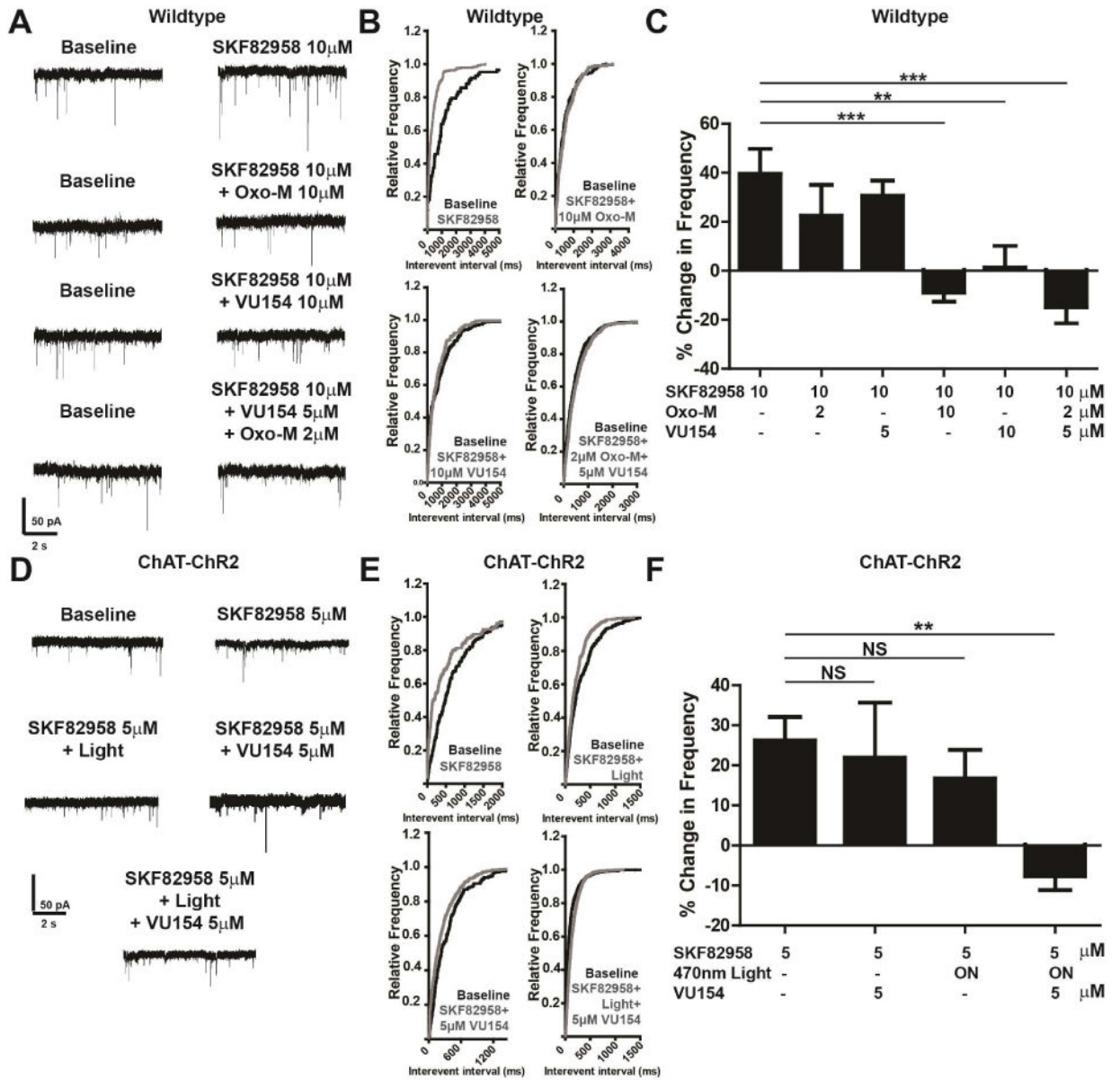
Figure 2. D$_1$ agonists increase GABA release in the SNr and this effect is reversed by muscarinic activation

A) Representative mIPSC traces from GABAergic cells of the SNr treated with 10 μM SKF82958 and 10 μM Oxotremorine-M (Oxo-M), 10 μM VU04567154, or 2 μM Oxo-M and 5 μM VU0467154 in wildtype (WT) mice. **B)** Cumulative probability plots of traces in **(A)**. **C)** Graph of data represented in **(A, B)**. Positive modulation corresponds to an increased mIPSC frequency and negative modulation corresponds to decreased mIPSC frequency as compared to baseline. **D)** Representative mIPSC traces from mice with channel rhodopsin 2 expressed under the choline acetyltransferase (ChAT-ChR2) promoter that were then optogenetically stimulated with 10 Hz 5 ms pulses of 470 nm light to release acetylcholine followed by treatment with 5 μM SKF82958, 5 μM M$_4$ PAM VU0467154, or a combination of these. **E)** Cumulative probability plots of traces in **(D). F)** Summary of data

represented in **(D, E).** Positive modulation corresponds to an increased mIPSC frequency and negative modulations correspond to decreased mIPSC frequency as compared to baseline. See also Figure S2, S3, and S4. Data are mean ± SEM with an n=8-11 per group in **(A-C)**, and n=8-14 per group in **(D-F)**. ** indicates p<0.01, *** indicates p<0.001, NS indicates not statistically significant by one way ANOVA followed by Tukey's post-hoc test.
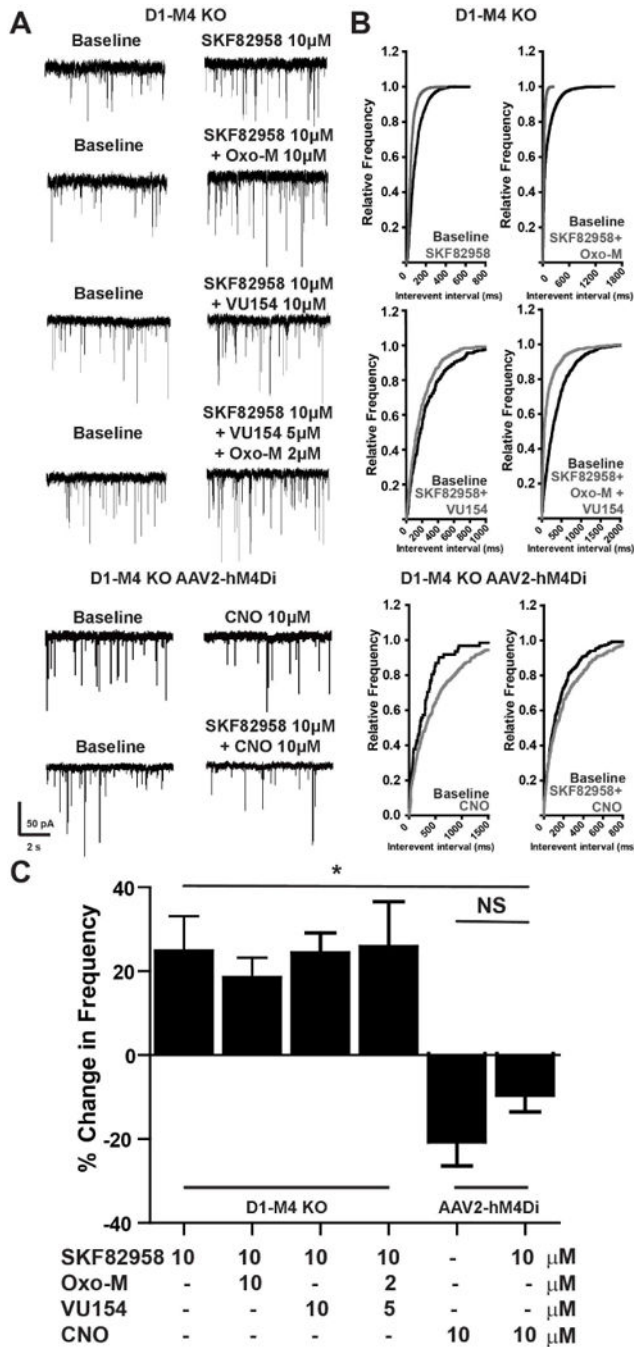
Figure 3. M$_4$ activation on D$_1$-SPN terminals in the SNr blocks D$_1$ evoked GABA release in the SNr

A) Representative mIPSC traces from GABAergic cells of the SNr in slices from D$_1$-M$_4$ KO mice treated with 10 μM SKF82958 and 10 μM Oxotremorine-M (Oxo-M), 10 μM VU04567154, 2 μM Oxo-M and 5 μM VU0467154, or from D$_1$-M$_4$ KO mice injected with AAV2-hM$_4$Di DREADD then treated with 10 μM SKF82958 and 10 μM CNO or CNO alone. **B)** Cumulative probability plots of traces in **(A)**. **C)** Summary of data represented in **(A, B)**. Positive modulation corresponds to an increased mIPSC frequency and negative

modulation corresponds to decreased mIPSC frequency as compared to baseline. See also Figure S4. Data are mean ± SEM with an n=8-10 per group. NS indicates not statistically significant by one way ANOVA followed by Tukey's post-hoc test.

Figure 4. M$_4$ receptor activity may tonically inhibit D$_1$-SPNs

A) Representative mIPSC traces recorded from GABAergic cells of the SNr from WT mice, mice that express Cre-recombinase under the D$_1$ promoter (D$_1$-Cre), or D$_1$-M$_4$ KO mice. **B)** Graph of baseline mIPSC frequency from **(A)**. **C)** Representative mIPSC traces from WT or D$_1$-M$_4$ KO from GABAergic cells of the SNr treated with 50 μM scopolamine, 1 μM of the highly selective M$_4$ antagonist mamba toxin-3 (MT-3), or 10 μM VU0467154 (VU154). **D)** Cumulative probability plots of traces in **(A)**. **E)** Summary of data represented in **(C, D)**. **F)** Representative images from ChAT-Cre animals then injected with an AAV control virus or

constitutively active caspase3 construct. Sections from the hindbrain were made and stained with an anti-vesicular choline acetyl transferase antibody and appropriate secondary antibody (green). Widefield images were taken using a 5X objective then stitched together. 20X images were taken on the border of the LDT and PPN to visualize both structures. Caspase3-injected animals showed fewer VAChT positive neurons than control virus-injected animals. **G)** Summary of *ex-vivo* electophysiological changes in mIPSC frequency from control or caspase3-injected ChAT-Cre animals after bath application of 1 μM MT-3. **H)** Graph of baseline mIPSC frequency from GABAergic cells of the SNr from control or caspase3-injected ChAT-Cre 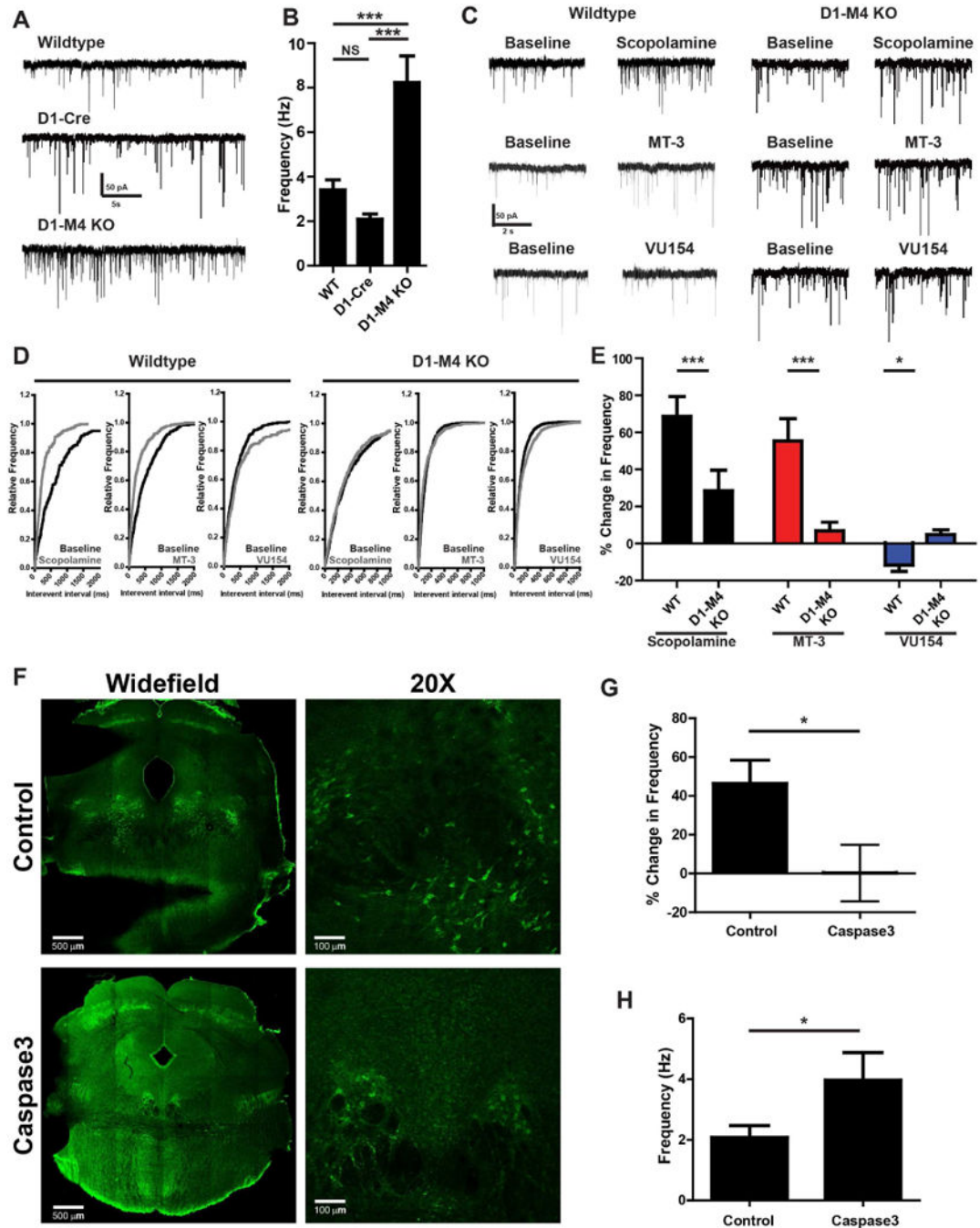animals. Positive modulation corresponds to an increased mIPSC frequency and negative modulation corresponds to decreased mIPSC frequency as compared to baseline. Data are mean ± SEM with an n=15-20 per group **(A, B)**, n=8-12 **(C-D)**, and n=6-8 **(C-D)**. *** indicates $p<0.001$ by one way ANOVA followed by Tukey's post-hoc test **(A, B)**, *** indicates $p<0.001$, * indicates $p<0.05$ by student's t-test in **(C-E)**, * indicates $p<0.05$ by Mann-Whitney test in **(F-H)**.
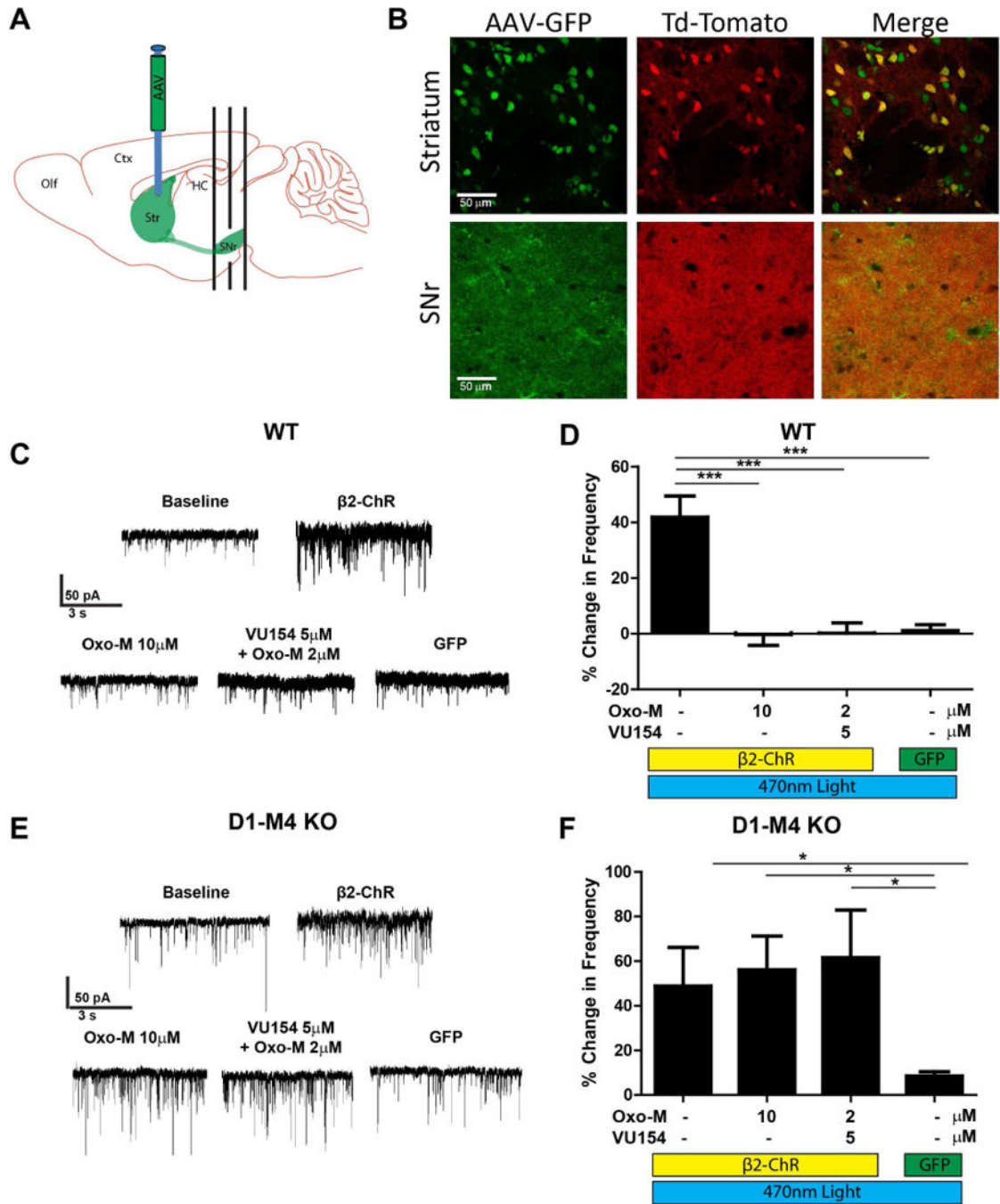
Figure 5. Adenylyl cyclase activation in D_1-SPN terminals mimics D_1 agonists and is blocked by M_4 activation

A) Diagram of AAV2-β2 Opto XR viral injection into the dorsolateral striatum and coronal sectioning technique of the SNr. **B)** Confocal microscopy images of mice with the fluorescent protein td-Tomato expressed under the D_1 promoter (D_1–td-Tomato, red) injected with AAV2-β2 Opto XR viral construct which has an enhanced yellow fluorescent protein (eYFP) reporter (green). While the expression of the viral construct is in both D_1 and non-D_1 structures in the striatum, due to sectioning technique, the viral construct (green) has

near complete co-localization (yellow) with the D_1 reporter (red) in the SNr. **C)** Representative mIPSC traces of GABAergic cells of the SNr from WT animals expressing the β2 Opto XR or eYFP control construct before and after optical stimulation and treatment with 10 μM Oxotremorine-M (Oxo-M) or 2 μM Oxo-M and 5 μM VU0467154. **D)** Summary of data represented in **(C)**. Positive modulation corresponds to an increased mIPSC frequency and negative modulation corresponds to decreased mIPSC frequency as compared to baseline. **E)** Representative mIPSC traces of GABAergic cells of the SNr from D_1-M_4 KO mice expressing the β2 Opto XR or eYFP control construct before and after optical stimulation and treated with 10 μM Oxotremorine-M (Oxo-M) or 2 μM Oxo-M and 5 μM VU0467154. **F)** Summary of data represented in **(E)**. Positive modulation corresponds to an increased mIPSC frequency and negative modulation corresponds to decreased mIPSC frequency as compared to baseline. See also Figure S5. Data are mean ± SEM with an n=8-10 per group **(C, D)** and n=8-14 per group **(E, F)**. * indicates p<0.05, ** indicates p<0.01, *** indicates p<0.001, NS indicates not statistically significant by one way ANOVA followed by Tukey's post-hoc test.

Figure 6. M$_4$ activity suppresses D$_1$ activation at the level of the SNr and may inhibit D$_1$ signaling in a synapse-specific manner

A) Structural T2- weighted magnetic resonance imaging (MRI) template images and cerebral blood volume (CBV) activation maps across 9 slices (caudal to rostral) of male Sprague-Dawley rats anesthetized and then treated with vehicle (intraperitoneal (i.p.), 10% Tween 80) or 30 mg/kg VU0467154 (i.p., 10% Tween 80) and then 1 mg/kg SKF82958 (i.p., sterile water). In the group activation maps, the red to yellow to red bar range represent increased CBV, indicating increased neuronal activity, while blue to purple color bar range represent decreased CBV, indicating decreased neuronal activity. **B-G)** Time courses and bar graphs of CBV changes after SKF82958 injection in rats pretreated with vehicle or M$_4$ PAM VU0467154 from indicated brain regions. Time course graphs show fractional changes in CBV, (CBV(t) over baseline (CBVo)) before SKF82958 injection, which was injected at minute 10. For the bar graphs, fractional CBV values were averaged between 20 to 30

minutes for each animal. See also Figure S6 and S7. Data are mean ± SEM with an n=6-8 per group. * indicates p<0.05, ** indicates p<0.01, *** indicates p<0.001, NS indicates non-significant by Wilcoxon matched pairs and rank test.

Author Manuscript
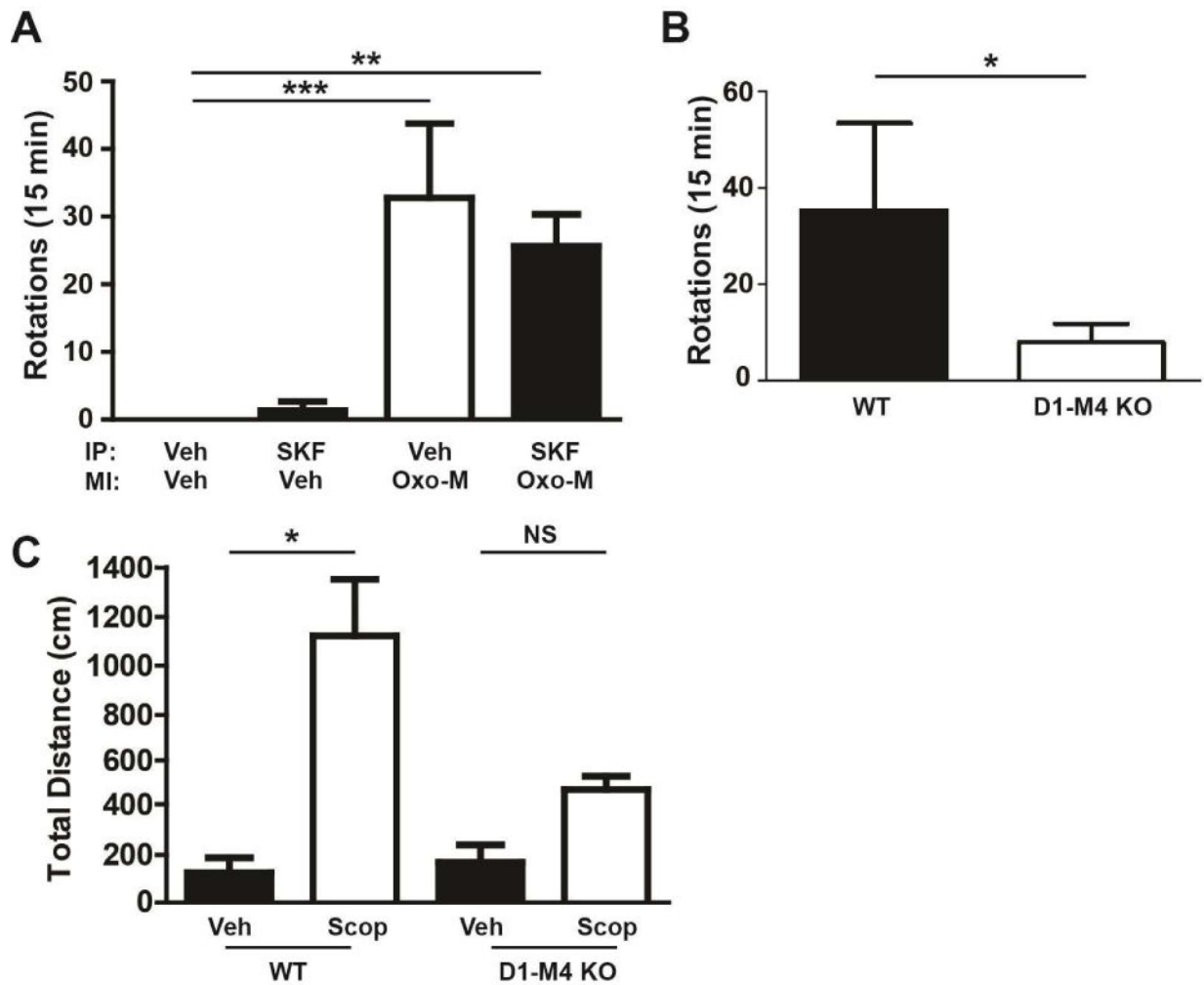
Author Manuscript

Author Manuscript

Author Manuscript

Figure 7. Muscarinic activation in the SNr is sufficient to block locomotion
A) WT mice were cannulated with the cannula sitting just above the SNr. Mice were pre-treated with the M_1 antagonist VU0255035 (3 mg/kg, intraperitoneal (i.p.), 10% Tween 80) to prevent the influence of M_1 activity on rotational behaviors 15 minutes prior to microinjection (MI). Mice were then injected in the SNr through the implanted cannula with 0.5 mg/ml of Oxo-M in 1 μL sterile water or 1μL sterile water alone. Animals that were injected with 0.3 mg/kg SKF89258 (i.p., sterile water) were injected 15 minutes prior to microinjection. Rotations were observed and scored by an experimenter blinded to conditions for 15 minutes after microinjection. Data represent total ipsilateral rotations. **B)** D_1-M_4 KO or littermate control mice that were cannulated in the SNr and microinjected with Oxo-M as in **(A)** and their rotations observed. **C)** WT or D_1-M_4 KO mice were bilaterally cannulated in the SNr and allowed to recover for 1 week. Mice were placed in an open field chamber and allowed to habituate for 90 minutes. After habituation, mice were bilaterally microinjected with 1 μL of 3 mg/ml scopolamine (sterile water) or sterile water alone. Data are shown as total distance traveled (cm) after microinjection. Data are mean ± SEM with an n=8 per group **(A)**, n=10-12 per group **(B)** and n=10-12 per group **(C)**. *

indicates p<0.05, ** indicates p<0.01 by Kruksal-Wallis test with Dunnett's compare all columns post-test.
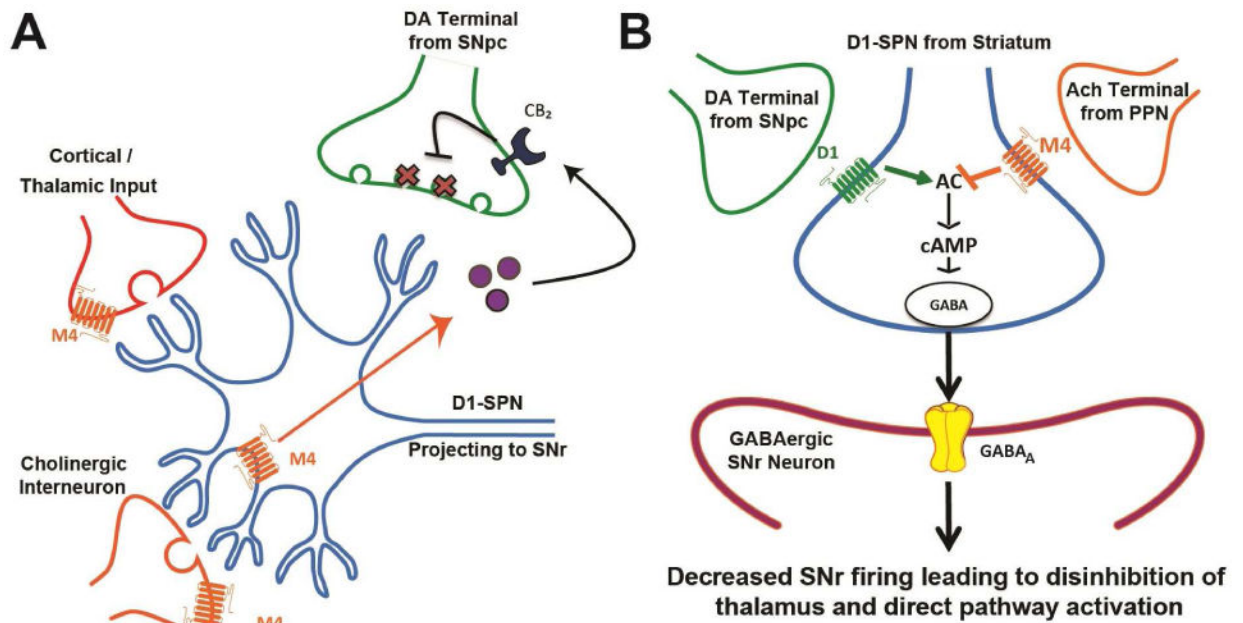
Figure 8. Model of D_1 and M_4 regulation of the direct pathway
A) M_4 activation in the striatum has complex actions on the circuitry of the basal ganglia. M_4 activation specifically on D_1-SPNs causes the release of an endocannabinoid (purple circles) which acts on cannabinoid receptor 2 (CB_2) receptors on DA terminals from the SNc to cause a sustained inhibition of DA release (X markers in DA terminals). In glutamatergic projections from the cortex and thalamus M_4 activation has been shown to decrease excitatory transmission and promote long term depression in the striatum. M_4 activation on cholinergic interneurons is suggested to decrease tonic firing and acetylcholine release. B) In the SNr, M_4 decreases GABA release probability through inhibiting AC and downstream cAMP signaling. Together, M_4 activation on D_1-SPNs in both the striatum and SNr are predicted to provide an efficient brake on D_1-SPN activity.